COST Action FP1402

„Basis of Structural Timber Design“

- from research to standard

Short Term Scientific Mission (STSM) Report

„Structural Analysis of In-plane Loaded CLT Beams with Holes or Notches“

by

Mario Jelec

University Josip Juraj Strossmayer of Osijek

Faculty of Civil Engineering Osijek

Osijek, Croatia

This STSM report covers research activities accomplished during the STSM from 1st September 2016 to 14th October 2016.

Host institution: Division of Structural Mechanics, Lund University, Sweden, prof. Erik Serrano

STSM Supervisor: Dr. Henrik Danielsson

1. Introduction

1.1. General

Cross laminated timber (CLT), being a versatile engineered timber product, has in recent years become well known and of global interests. CLT presents a two dimensional plate-like laminated prefabricated product, in general composed of an uneven number of orthogonally bonded layers which are made of side by side placed boards and arranged crosswise to each other at an angle of 90°. Due to its crosswise orientation, CLT is capable of carrying both in- and out-of-plane loads and can be used for wall or floor elements as well as for linear members. For CLT under out-of-plane loading (e.g. floor elements) test configurations and strength values are well agreed upon and several design procedures are proposed in design handbooks and technical provisions (Brandner et al., 2016). For CLT under in- plane loading (e.g. wall elements or beam elements), some properties and failure modes such as in-plane shear strength are still under discussion, presently resulting in conservative regulations (Brandner et al., 2016). A major obstacle for developers, producers and designers is the current status of CLT in European product and standard design, since properties and design for CLT have been regulated via national or international European Technical Approvals (ETAs). A product standard for CLT, EN 16351 (2015) has recently been published, but CLT is still not included in the European timber design code Eurocode 5 (EC5, 2004).

1.2. Background

CLT elements under in-plane loading, such as CLT beams, offer several advantages over solid or glued laminated timber beams due to their specific layup of orthogonally bonded layers. This is especially emphasized in applications where tensile stresses perpendicular to the beam axis are critical for the load carrying capacity, e.g. notched beams or beams with holes. In such beams, made of glulam or sawn timber, crack initiation is followed by crack opening and propagation at the two corners exposed to tensile stresses perpendicular to the grain. Since the perpendicular to grain tensile strength is very low, this stress situation results in general in much lower load carrying capacity compared to the capacity of timber beams without holes or notches. In the case of reinforcement using screws or wood based panels, the load bearing capacity can be increased for the areas around a hole or a notch, but in cases when nearly the whole timber member needs to be reinforced their efficiency can be questionable. In that case, CLT beams present a much better solution thanks to its lay-up where tensile forces perpendicular to the beam axis can be transferred by the transversal layers and additional reinforcement is generally not needed.

Design of timber elements with holes or notches are treated differently in existing timber design codes. At present, the European timber design code (EC5, 2004) does not contain any design rules for holes in glulam or other engineered wood products. The German National Annex to Eurocode 5, DIN EN 1995-1-1 (2012) as well as Austrian National Annex, ÖNORM B 1995-1-1 (2014) contain equations and recommendations for both unreinforced and reinforced glulam and solid wood members. Due to the fact that CLT beams with holes or notches are characterized by different failure mechanisms compared to glulam or solid timber beams and that some of the proposed equations in the standards are derived from parameter studies based on FE-analysis carried out on solid timber beams, it is questionable whether they should be used at all for the case of CLT beams. The proposed equations and recommendations in the standards are based on a large number of so far carried out experimental tests, see e.g. (Danielsson, 2007) for a review of tests, as well as on principles of theoretical and numerical analysis based in some cases on different approaches based on fracture mechanics (Serrano, 2016). In case of CLT beams with holes or notches, until now experimental test has been carried out only by Flaig (2013). Except experimental results, Flaig (2013) proposed analytical models for CLT beams without holes or notches, as well as for CLT beams with holes or notches (Flaig, 2014). Numerical analysis based on 3D FE-models (Jelec at al., 2016) showed in general good agreement with Flaig´s model in case of CLT beams without holes or notches. Slightly larger differences were found for the case of CLT beams with holes, where the FE-analysis suggests a slightly more favorable stress situation compared to Flaig’s model. Since Flaig´s experimental work was conducted on a limited number of specimens of a specific “ideal” lay-up (which will be explained in more detail below), further experimental work on more “standard” lay-up is needed in first step for validation as well as for further development of existing model.

1.3. Aim of STSM

The main purpose of this Short Term Scientific Mission is to investigate the structural behavior of CLT beams with holes or notches loaded in plane under various loading conditions and different cross section lay-up. The STSM is aimed at giving additional contribution to the ongoing review process of Eurocode 5, regarding CLT beams in these specific applications. Special emphasis is on shear loading and in-plane shear behavior considering the complex internal structure of CLT beams. In that sense, the main contribution of the mission are the experimental test results obtained on a total of 20 CLT beams divided into 5 different test series. The results represent a considerable and valuable contribution, since except Flaig´s test results, they represent the only available test data considering CLT beams with holes or notches. Also, this mission represents a starting point for further collaboration between the participating institutions, a collaboration that will be based on further 3D numerical and analytical analysis, as well as on more extended experimental work in the near future.

1.4. Content of this report

The report is organized in the following way. After this short introduction, the first part is based on existing analytical models for the case of CLT beams without holes or notches, as well as for the case of beams with holes or notches. The main features of the model, including restrictions and background theory, are explained and critical stresses for each failure mode in the CLT beams are presented. The second and main part of the report contains experimental results, with detailed explanation of tested specimens and measuring data. In this part, the main results are presented including graphs, photos and stress calculations for failure loads obtained from testing. The third and last part contains preliminary conclusions based on the experimental results, comparison with Flaig´s analytical model and equations from standards (EC5/NA) as well as recommendations and plans for further future work.

2. Analytical model of CLT beams loaded in- plane

2.1. Failure modes

In CLT beams exposed to in-plane loading, normal and shear stresses occur. In verification of normal stresses, only bending resistance of the net cross section area is taken into account, here meaning layers with boards oriented in the direction of stress (Schickhofer et al. 2010). The contribution of transversal layers (α=90°) is neglected due to high ratio of MOE, typically with $E_0/E_{90} \approx 30\text{-}40$. In verification of shear strength, according to Bogensperger et al. (2007, 2010), Flaig and Blass (2013) and Brandner et al. (2013) three different shear failure mechanism have to be considered, depending on existence of adhesive bonding of the narrow faces (Fig. 1):

- Failure mode I (FM I) or **gross shear failure** of the CLT element by shear failure in all layers, normally only relevant for elements with narrow face bonding
- Failure mode II (FM II) or **net shear failure** of the CLT element by shear failure in the net cross section of the element (where the layers with the smallest value of the total thickness of longitudinal and transversal layers, respectively, being decisive in the case of equal material properties in all layers)
- Failure mode III (FM III) or **shear failure in the crossing areas** between orthogonally bonded lamellae involving torsional and unidirectional shear stresses

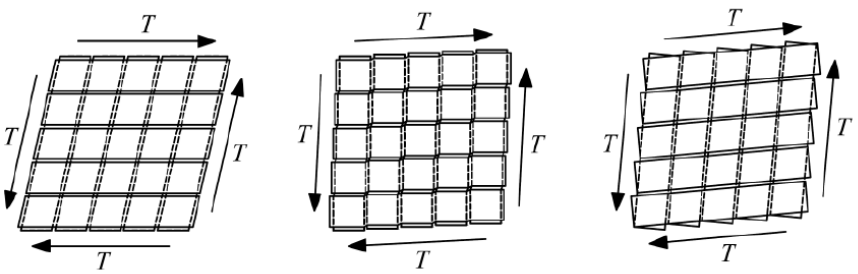

Figure 1. Failure modes I, II and III in CLT-beams subjected to transversal forces in plane direction (from left to right), (Flaig, 2013)

2.2. Analytical approach for CLT beams without holes or notches

For evaluation of shear stresses in CLT elements loaded in-plane, two different models are proposed. In case of a CLT wall element loaded in-plane and considering uniform stress loading on wall boundaries, an efficient mechanical model for internal stress verification has been evaluated by Moosbrugger et al. (2006) and Bogensperger (2007, 2010). The evaluated method is based on an elementary representative volume sub element (RVSE), which represents the smallest unit cell at intersection between two orthogonal boards whose internal stress state describes the global behavior of the CLT element (Fig. 2). Verification of shear stresses includes in total three components of shear stresses: net shear stresses in longitudinal layers, net shear stresses in transversal layers and torsional shear stresses in crossing areas. Since this model is intended more for CLT walls, its further evaluation and explanation is omitted in this report.

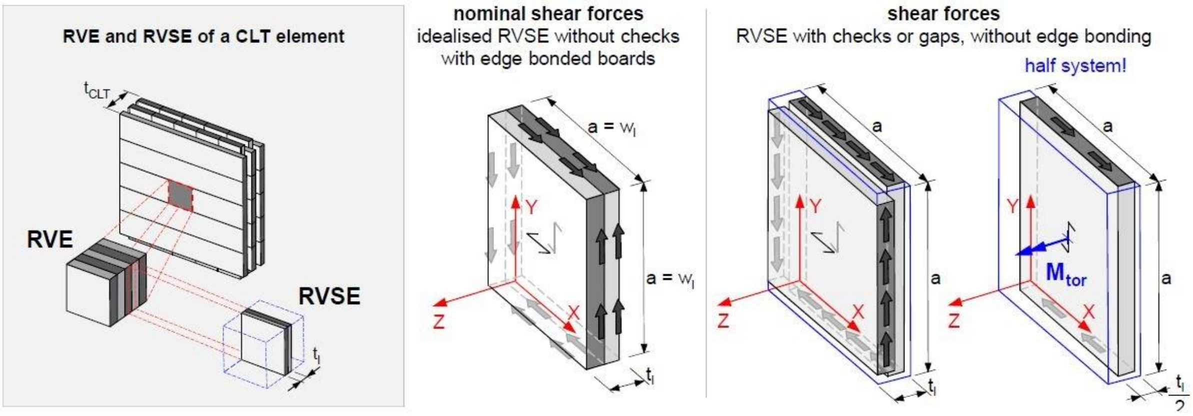

Figure 2. Representative volume sub element (RVSE) for verification of shear stresses in CLT wall elements (Bogensperger, 2007)

For CLT beams exposed to both bending and shear loading Flaig (2013) proposed a design procedure based on the theory of composite beams for verification of shear stresses. In case of FM I and FM II, shear stresses τ_{xy}, causing failure parallel and perpendicular to the grain, can be evaluated using Bernoulli-Euler beam theory using the following expressions:

$$\tau_{xy,gross} = \frac{V_y \cdot S_{z,gross}}{I_{z,gross} \cdot t_{gross}} \qquad \text{(FM I)} \tag{1}$$

$$\tau_{xy,net} = \frac{V_y \cdot S_{z,net}}{I_{z,net} \cdot t_{net}} \qquad \text{(FM II)} \tag{2}$$

where V_y is the shear force, S_z is the static moment about z-axis, I_z is the second moment of inertia about z-axis, t_{gross} is the total thickness of the CLT beam and t_{net} is the net section thickness of the CLT beam. Index *gross* refers to the complete/total cross section and *net* refers to the total thickness of the layers of either the longitudinal or the transversal layers only. For the common case of equal strength properties of the transversal and longitudinal layers, the strength with respect to FM II is limited by the strength of the layers (longitudinal or transversal) with the smallest total thickness t_{net}.

Maximum values can be evaluated as peak values of the parabolic functions according to Eq. 3 and 4 (Fig. 3 and Fig. 4).

$$\tau_{xy,gross,max} = 1{,}50 \cdot \frac{V_y}{h \cdot t_{gross}} \quad \text{(FM I)} \tag{3}$$

$$\tau_{xy,net,max} = 1{,}50 \cdot \frac{V_y}{h \cdot t_{net}} \quad \text{(FM II)} \tag{4}$$

An example of shear stress distribution along the longitudinal and transversal layers of CLT beam, with four lamellae in the longitudinal layers, is shown in Fig. 3 and with three lamellae in the longitudinal layers in Fig. 4, respectively. The illustrations in both these figures represent the stress distribution at a cross section through the center of a transverse lamella. According to Flaig (2013), and in case of an even number of lamellae in the longitudinal layers, Eq. 3 overestimates the maximum shear stress in the gross cross section (Fig. 3), whereas in case of an odd number of lamellae in the longitudinal layers, the maximum net shear stresses are overestimated by Eq. 4 (Fig. 4). For the cross section depicted in Fig. 3 the difference is 6.3 % and for the cross section in Fig. 4 it is 11 %. However, the error decreases rapidly with an increasing number of lamellae in the longitudinal layers (Flaig, 2013).

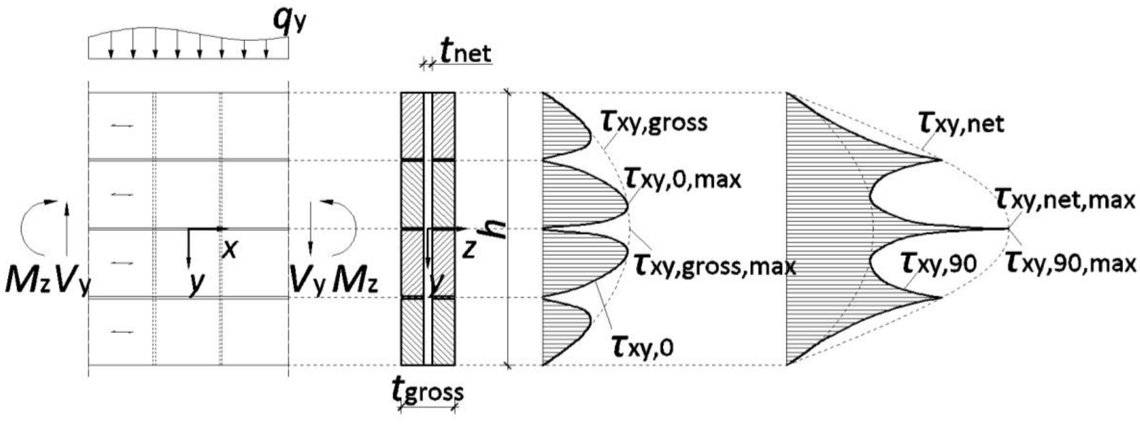

Figure 3. Distribution of shear stresses in the lamellae of CLT beam with four longitudinal lamellae: shear stresses $\tau_{xy,0}$ in longitudinal lamellae (left) and shear stress $\tau_{xy,90}$ in transversal lamellae (right)

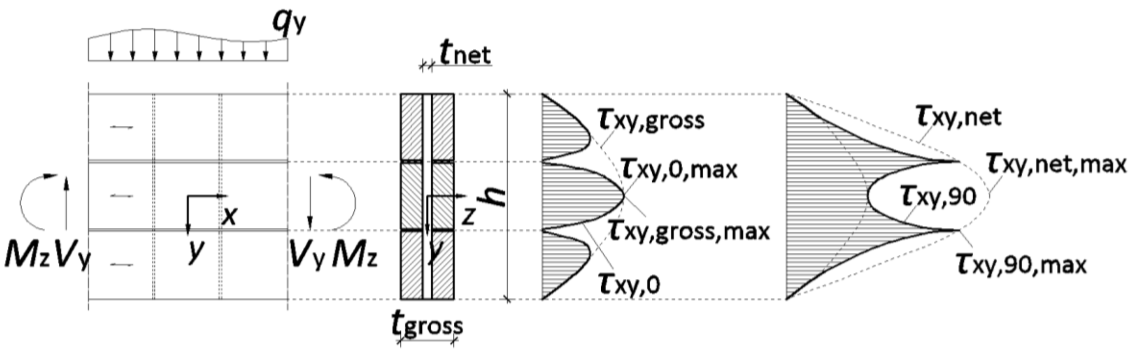

Figure 4. Distribution of shear stresses in the lamellae of CLT beam with three longitudinal lamellae: shear stresses $\tau_{xy,0}$ in longitudinal lamellae (left) and shear stress $\tau_{xy,90}$ in transversal lamellae (right)

In the case of FM III, in total three components of shear stress participate in load transfer within the crossing areas between the orthogonally bonded lamellae (Flaig, 2013): shear stresses parallel to the beam axis (τ_{zx}), torsional shear stresses (τ_{tor}) and shear stresses perpendicular to the beam axis (τ_{zy}).

The shear stresses parallel to the beam axis, τ_{zx}, are caused by the variation in the bending moment as a function of the x-coordinate and are evaluated using a composite beam model. The maximum value of the stresses is found at the outermost lamellae of the beam and this corresponds well with numerical results based on 3D FE-analysis by Jelec et al. (2016). The maximum value of the shear stress parallel to the beam axis can be calculated according to:

$$\tau_{zx} = \frac{6V_y}{b^2 \cdot n_{CA}} \cdot \left(\frac{1}{m^2} - \frac{1}{m^3}\right) \tag{5}$$

where b is the width of lamellae, n_{ca} is the number of crossing areas within the beam thickness and m is the number of longitudinal lamellae within the beam height.

Torsional stresses, τ_{tor}, arise due to the eccentricity between the center lines of adjacent lamellae and they are also derived using the composite beam model. In the work presented by Flaig, equal torsional moments, and hence equal torsional shear stresses, are assumed for all crossing areas in the beam height direction, based on the condition that the lamellae in the transversal layers are assumed to remain straight in the deformed beam. From numerical analysis based on 3D FE-models (Jelec et al. 2016) it seems like torsional moments, as well as torsional stresses are higher in the crossing areas close to the neutral axis and lower at crossing areas closer to the upper and lower side of the beam. According to the model by Flaig, assuming equal torsional moments for all crossing areas in the beam height direction, the maximum torsional shear stress can be calculated according to:

$$\tau_{tor} = \frac{3V_y}{b^2 \cdot n_{CA}} \cdot \left(\frac{1}{m} - \frac{1}{m^3}\right) \tag{6}$$

According to Flaig (2013), Eq. 5 and Eq. 6 provide accurate results for CLT beams with constant ratio $t_{long,k}/n_{ca,k}$ between the thickness of an individual longitudinal layer and the number of glue lines the respective layer shares with adjacent transversal layers. In that case, shear stresses τ_{zx} and τ_{tor} are constant across the beam thickness. Hence, Eq. 5 and Eq. 6 are derived based on an "ideal" cross section lay-up (e.g. obtained by using double centric layers of boards of equal thickness as for the outer longitudinal layers or using a centric layer of boards with twice the thickness of the boards in the outer longitudinal layers). However, within the range of layups that are used in practice, the variation of shear stresses τ_{zx} and τ_{tor} is small, especially for CLT beams made of softwood, with MOE of the lamellae around 11 000 N/mm² (Flaig, 2013). In this report, the same equations are used for the evaluation of the experimental results obtained in Lund, which were carried out on "standard" CLT beams with a cross section lay-up composed of boards of equal thickness for all longitudinal layers and hence not a constant ratio $t_{long,k}/n_{ca,k}$. This issue will be further investigated in future publications.

Shear stresses perpendicular to the beam axis, τ_{zy}, arise due to external loads, e.g. support reactions or external forces, or close to holes or notches. For a CLT beam without a hole or a notch, and exposed to an external force q_y [N/m] applied to the end grain of the transversal layers, shear stresses can be evaluated according to Eq. 7 (Flaig, 2015).

$$\tau_{zy} = \frac{q_y}{m \cdot b \cdot n_{CA}} \tag{7}$$

In the design of CLT beams, each of the stress components must be verified with the corresponding shear strength related to a relevant shear failure mode. Also, in the crossing areas, interaction of shear stresses has to be considered. According to Flaig (2013) for verification of FM III, two interactions have to be considered:

$$\frac{\tau_{zx}}{f_R} + \frac{\tau_{tor}}{f_{tor}} \leq 1{,}0 \quad (\text{FM III} - \text{A}) \tag{8}$$

$$\frac{\tau_{zy}}{f_R} + \frac{\tau_{tor}}{f_{tor}} \leq 1{,}0 \quad (\text{FM III} - \text{B}) \tag{9}$$

where f_R is the rolling shear strength and f_{tor} is the torsional strength.

2.3. Analytical approach for CLT beams with holes

For analysis of CLT beams with holes, Flaig (2014) derived stress concentration factors by performing numerical parameter studies on girder FE- models where longitudinal and transversal lamellae were represented by Timoshenko beam elements connected to each other by rotational and translational spring elements. Since the parameter study was comprehensive, some idealizations were introduced. Analysis was done on “ideal” cross section lay-up, using double centric layer as explained earlier. In all simulated CLT beams, the width *b* of the longitudinal and transversal lamellae was set to 150 mm and ratios of t_{net}/t_{gross} = 0.20 and t_{gross}/n_{ca} = 50 mm were constantly used. By using regression analysis, for all simulated beams the ratios k_{h1} and k_{h2}, representing ratios of maximum shear stresses at the hole to shear stress in an undisturbed beam of equal dimensions, were derived (Eq. 10 and Eq. 11).

$$k_{h1} = \frac{\tau_{tor,h}}{\tau_{tor}} = \left[1.81 \cdot \left(\frac{l_h}{h} \cdot \frac{h_h}{h - h_h}\right) + 1.14\right] \tag{10}$$

$$k_{h2} = \frac{\tau_{zx,h}}{\tau_{zx}} = \left[103 \cdot \left(\frac{h_h \cdot l_h}{h^2} \cdot m^2\right) + 1.27\right] \tag{11}$$

where l_h is hole length and h_h is hole height.

For verification of normal stresses due to bending, both the capacity of the complete cross section with respect to the maximum bending moment (Eq. 12) and the capacity of the reduced cross section at the hole (Eq. 13 and Eq. 14) need to be considered. In both cases, stresses are calculated considering the bending resistance of the longitudinal layers only.

$$\sigma_{m,net} = \frac{M_{max}}{W_{net}} = \frac{6 \cdot M_{max}}{t_{net,0} \cdot h^2} \tag{12}$$

$$\sigma_{m,net,h,t} = \frac{M_h}{\mathrm{W}_{net,h}} + \frac{M_V}{W_{net,h,t}} \tag{13}$$

$$\sigma_{m,net,h,b} = \frac{M_h}{\mathrm{W}_{net,h}} + \frac{M_V}{W_{net,h,b}} \tag{14}$$

$$M_V = \frac{V}{2} \cdot \frac{l_h}{2} \tag{15}$$

$$W_{net,h,t} = \frac{t_{net,0} \cdot h_{r,top}^2}{6} \tag{16}$$

$$W_{net,h,b} = \frac{t_{net,0} \cdot h_{r,bottom}^2}{6} \tag{17}$$

where M_{max} is the maximum bending moment, W_{net} is the net section modulus including only longitudinal layers, $t_{net,0}$ is the net thickness of longitudinal layers, M_h is the bending moment at the center of the hole, M_V is the additional bending moment at the edge of the hole (caused by shear force $V/2$ and lever arm $l_h/2$ giving a local bending of the beam part above and below the hole), $W_{net,h,t}$ is the net section modulus including only the part of the beam above the hole, $W_{net,h,b}$ is the net section modulus including only the part of the beam below the hole, $h_{r,top}$ is residual beam height above the hole and $h_{r,bottom}$ is residual beam height under the hole. The calculation of the additional bending moment M_V in Eq. 15 is based on an assumption of a hole which is centrically placed with respect to the beam height direction giving an equal distribution of the shear force between the beam parts above and below the hole, respectively.

According to the Austrian NA to EC5 (2014), the verification of the bending moment capacity at the holes should be carried out slightly different compared to Eq. 13 and Eq. 14 above. Instead of using M_h as the bending moment at the center of the hole, the Austrian NA suggests to use the value of the bending moment at the edge of the hole and also take into account the additional bending moment M_V as given in Eq. 15. This approach appears to be in disagreement with the underlying beam theory and equilibrium conditions and is also not in agreement with (Erläuterungen zur DIN 1052:2004-08), describing background and application of the previous German code DIN 1052.

The tensile forces perpendicular to the beam axis at the vertical edges of the holes were calculated according to Eq. 18 which is given in German and Austrian NA to EC5 for glulam beams with holes.

$$F_{t,90} = F_V + F_M = V_y \cdot \left[\left(\frac{3h_h}{4h} - \frac{h_h^3}{4h^3}\right) + \left(\frac{0.008 \cdot x_h}{h_r}\right)\right] \tag{18}$$

where $h_r = \min\{h_{r,top}; h_{r,bottom}\}$ and x_h is the distance between support and the furthest edge of the hole.

Tensile stresses in transversal lamellae at the edges of the holes were calculated using an effective width a_r, which is chosen as the smaller value of the actual width of the first vertical lamellae at the hole and the maximum value given in the German/Austrian NA to EC5 for glulam beams with external reinforcement (Eq. 19). The highly non-uniform distribution of the tensile stresses is accounted for in the German NA with a factor k_k = 2.0, giving the following expression for the tensile stress perpendicular to the beam axis.

$$\sigma_{t,90} = k_k \cdot \frac{F_{t,90}}{a_r \cdot t_{net,90}} \tag{19}$$

where $a_r = \min\{b\,;0.3(h+h_h)\}$ and $t_{net,90}$ is total thickness of the transversal layers.

In the evaluation of shear stresses, verification of all three failure modes have to be considered, i.e. shear stress in the gross cross section (FM I), shear stresses in the net cross section (FM II) and shear stresses in the crossing areas (FM III). The following equations have to be calculated:

$$\tau_{xy,gross,h} = 1{,}5 \cdot \frac{V_y}{(h-h_h)\cdot t_{gross}} \quad \text{(FM I)} \tag{20}$$

$$\tau_{xy,net,h} = k_{h2} \cdot \tau_{xy,net,max} = k_{h2} \cdot 1{,}50 \cdot \frac{V_y}{h \cdot t_{net}} \quad \text{(FM II)} \tag{21}$$

$$\tau_{tor,h} = k_{h1} \cdot \tau_{tor} = k_{h1} \cdot \frac{3V_y}{b^2 \cdot n_{CA}} \cdot \left(\frac{1}{m} - \frac{1}{m^3}\right) \tag{22}$$

$$\tau_{zx,h} = k_{h2} \cdot \tau_{zx} = k_{h2} \cdot \frac{6V_y}{b^2 \cdot n_{CA}} \cdot \left(\frac{1}{m^2} - \frac{1}{m^3}\right) \tag{23}$$

$$\tau_{zy,h} = \frac{F_{t,90}}{n_{CA} \cdot a_r \cdot h_r} \tag{24}$$

According to Flaig (2013) for verification of FM III, two interactions have to be considered:

$$\frac{\tau_{zx,h}}{f_R} + \frac{\tau_{tor,h}}{f_{tor}} \leq 1{,}0 \quad \text{(FM III} - \text{A)} \tag{25}$$

$$\frac{\tau_{zy,h}}{f_R} + \frac{\tau_{tor,h}}{f_{tor}} \leq 1{,}0 \quad \text{(FM III} - \text{B)} \tag{26}$$

where f_R is the rolling shear strength and f_{tor} the torsional strength.

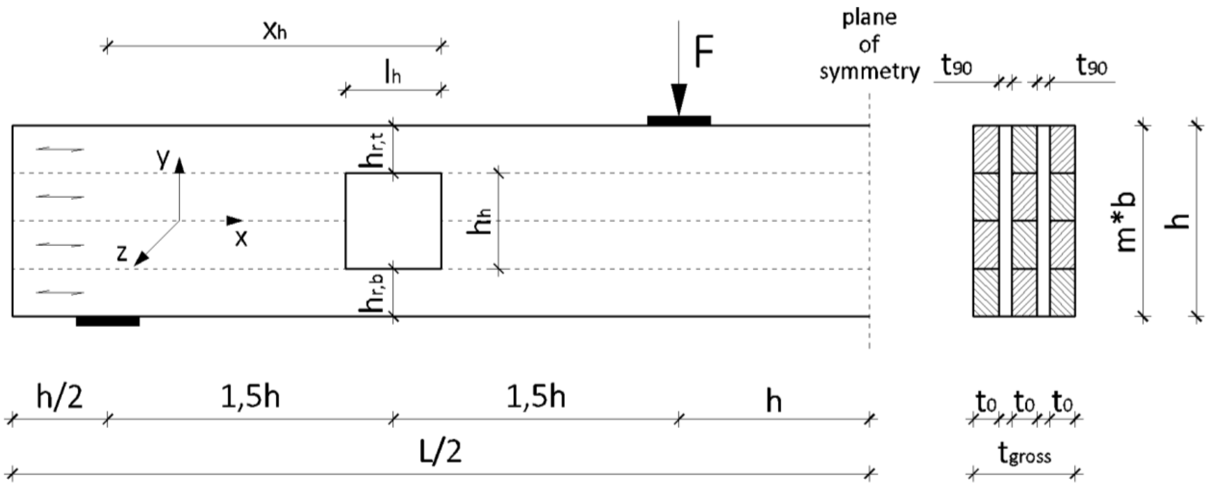

Figure 5. Geometry, layup and labels of tested CLT beam with hole

2.4. Analytical approach of notched CLT beam

For the verification of notched CLT beams, Flaig (2014) derived stress concentration factors by using the same type of girder FE-model with the same assumptions and idealizations used for the case of CLT beams with holes. Since in all simulated beams the shear stress component parallel to the beam axis in the crossing areas at the corner of the notch τ_{zx} was smaller than the maximum shear stress component perpendicular to the beam axis, determination of a stress concentration factor for the shear stress component parallel to the beam axis is omitted (Flaig, 2014). For all simulated beams, the ratio k_h between maximum torsional shear stress in the corner of the notch and the corresponding value in the beam without the notch was evaluated according to Eq. 27 and Eq. 28 by means of a regression analysis.

$$k_n = 0{,}877 \cdot \left(\frac{h_{ef}}{h}\right)^{k_c} \tag{27}$$

$$k_c = -1{,}81 \cdot \left(\frac{c}{h}\right)^{0{,}479} \tag{28}$$

where c is the distance between support and notch face and h_{ef} is the residual height of the beam at the notch.

For verification of normal stresses due to bending, both the capacity of the complete cross section with respect to the maximum bending moment (Eq. 29) and the capacity of the reduced cross section at the notch (Eq. 30) need to be considered. In both cases, stresses are calculated considering the bending resistance of the longitudinal layers only.

$$\sigma_{m,net} = \frac{M_{max}}{W_{net}} = \frac{6 \cdot M_{max}}{t_{net,0} \cdot h^2} \tag{29}$$

$$\sigma_{m,net,n} = \frac{M_n}{W_{net}} = \frac{6 \cdot M_n}{t_{net,0} \cdot h_{ef}^2} \tag{30}$$

where M_n is the bending moment at the corner of the notch.

The tensile force perpendicular to the beam axis at the notch was calculated according to Eq. 31 which is given in German NA to EC5 in relation to design of reinforcement of notched glulam beams.

$$F_{t,90} = 1{,}3 \cdot V_y \cdot \left[3 \cdot \left(1 - \frac{h_{ef}}{h}\right)^2 - 2 \cdot \left(1 - \frac{h_{ef}}{h}\right)^3\right] \tag{31}$$

Tensile stresses in the first transversal lamellae at the notch were calculated using an effective length l_r, which is chosen as the higher value of the actual width of the first transversal lamellae at the notch and the maximum value given in German NA to EC5 for notched glulam beams with external reinforcement (Eq. 32). The highly non-uniform distribution of the tensile stresses is accounted for in the German NA with a factor k_k = 2.0, giving the following expression for the tensile stress perpendicular to the beam axis.

$$\sigma_{t,90} = k_k \cdot \frac{F_{t,90}}{l_r \cdot t_{net,90}} \tag{32}$$

where $l_r = \max\{b\,;0.5(h - h_{ef})\}$.

As for beams with holes the shear stresses related to the three failure modes have to be considered, i.e. shear stress in the gross cross section (FM I), shear stresses in the net cross section (FM II) and shear stresses in the crossing areas (FM III). The following equations have to be calculated:

$$\tau_{xy,gross,n} = 1{,}50 \cdot \frac{V_y}{h_{ef} \cdot t_{gross}} \quad \text{(FM I)} \tag{33}$$

$$\tau_{xy,net,n} = k_n \cdot \tau_{xy,net,max} = k_n \cdot 1{,}50 \cdot \frac{V_y}{h \cdot t_{net}} \quad \text{(FM II)} \tag{34}$$

$$\tau_{tor,n} = k_n \cdot \tau_{tor} = k_n \cdot \frac{3V_y}{b^2 \cdot n_{CA}} \cdot \left(\frac{1}{m} - \frac{1}{m^3}\right) \tag{35}$$

$$\tau_{zy,h} = \frac{F_{t,90}}{n_{CA} \cdot l_r \cdot h_n} \tag{36}$$

where $h_n = \min\{h_{ef}; h - h_{ef}\}$

According to Flaig (2014) for verification of FM III, interactions between torsional shear stresses and shear stresses perpendicular to the beam axis have to be calculated.

$$\frac{\tau_{\mathrm{zy,n}}}{f_R} + \frac{\tau_{\mathrm{tor,n}}}{f_{tor}} \leq 1{,}0 \quad (\mathrm{FM\ III} - \mathrm{B}) \tag{37}$$

where f_R is the rolling shear strength and f_{tor} the torsional strength.

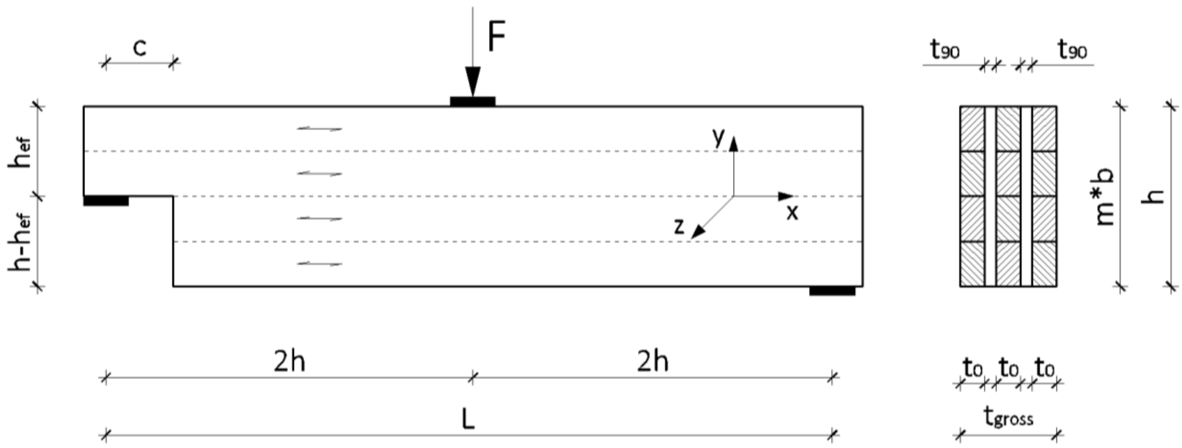

Figure 6. Geometry, layup and labels of tested notched CLT beam

3. Experimental program of CLT beams loaded in-plane

3.1. Introduction

The experimental program presented in this report deals with the strength of CLT beams loaded in-plane. A total of 20 individual tests were carried out, divided into five test series with four nominally equal tests in each test series. Two test series consisted of CLT beams without holes or notches, two test series consisted of CLT beams with a hole and one test series consisted of notched CLT beams. In all test series, cross section dimensions and layup of cross sections were kept the same. For the CLT beams with a hole, all holes were square without rounded corners, placed centrically with respect to the beam height and with a side length equal to a half of the beam height. In case of CLT beams without holes or notches, one test series was designed for verification of bending strength while the other one was designed for verification of shear strength. In case of the test series of CLT beams with a hole, in one of the setups the holes are placed in a position of a combined state of shear force and bending moment while in the other setup the holes are placed with its center in a point of zero bending moment. Beams with a hole placed in a position of zero bending moment seem to never have been investigated before, since in Flaig´s experimental tests all holes were positioned in regions of combined state of shear force and bending moment. In addition, Flaig´s experimental tests were carried out with cross sections with double centric layers, or as previously referred to as “ideal” cross section layup. Although appealing from a research point of view, this type of “ideal” layup is generally not used in practice. For all tests carried out in Lund, a more conventional cross section layup was used with a total of five layers and with equal width of the boards within the three longitudinal layers.

3.2. Test series

The test series are in Table 1 described concerning name, number of tests, beam size, beam span, hole and notch size and lay-up. The geometric properties and the bending moment to shear force ratios at the hole are presented in Figure 7. Test series A represents CLT beams with a hole in a position of combined state of shear force and bending moment (M/V = 1.5 h), while test series B represents CLT beams with a hole in a position of pure shear force, with zero bending moment in the center point of the hole (M/V = 0). Test series C represents CLT beams without holes or notches, designed for verification of bending strength, while in test series E beam span was reduced to avoid premature bending failure and instead provoke shear failure of the CLT beams. Test series D represents notched CLT beams.

Table 1. Test series

Test series	**Number of tests**	**Beam size** t_{gross} **x** h **[mm²]**	**Beam span** L **[mm]**	**Hole size** l_h **x** h_h **[mm²]**	**Notch size** h_{ef} **x** c **[mm²]**	**Lay-up**
A	4	160 x 600	4800	300 x 300	-	l-c-l-c-l
B	4	160 x 600	3000	300 x 300	-	l-c-l-c-l
C	4	160 x 600	4800	-	-	l-c-l-c-l
D	4	160 x 600	2400	-	-	l-c-l-c-l
E	4	160 x 600	2400	-	300 x 200	l-c-l-c-l

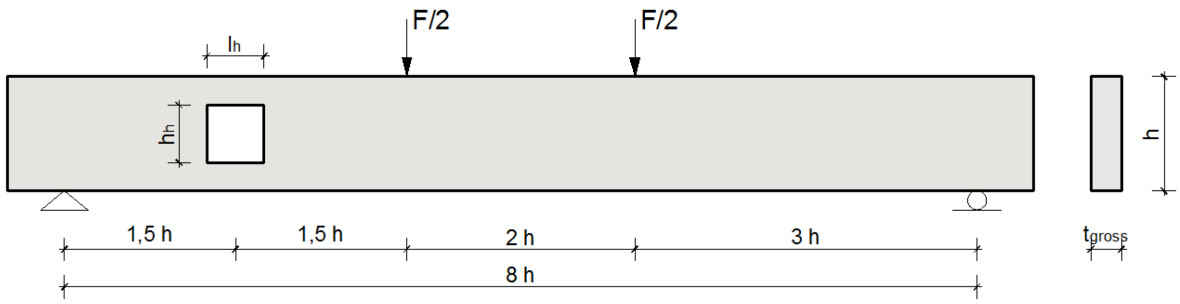

Figure 7. Geometry properties and test setup of test series A

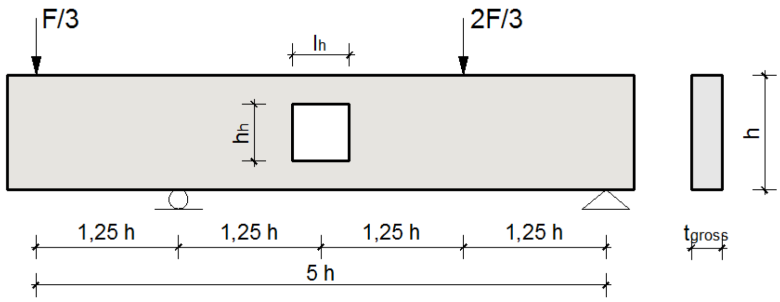

Figure 8. Geometry properties and test setup of test series B

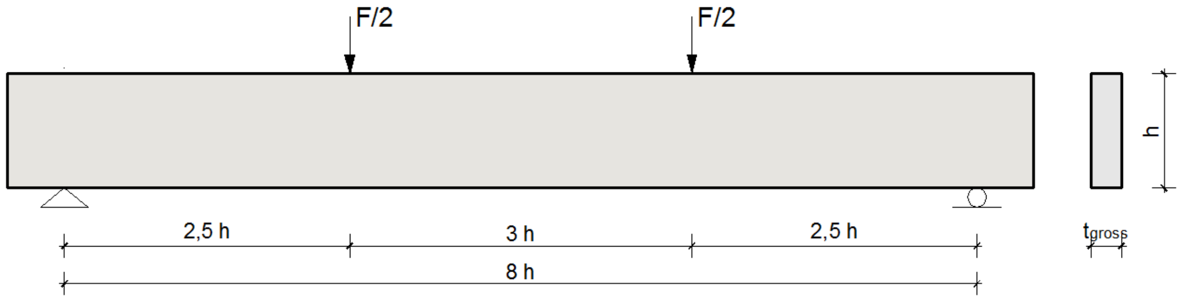

Figure 9. Geometry properties and test setup of test series C

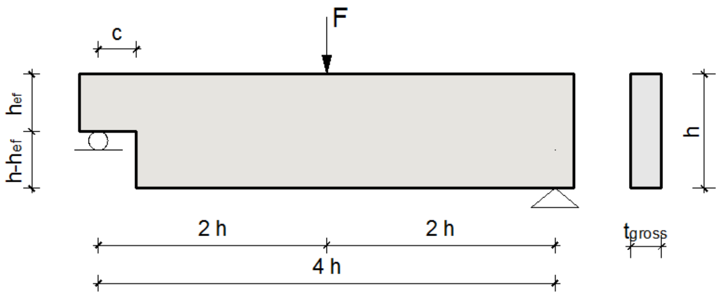

Figure 10. Geometry properties and test setup of test series D

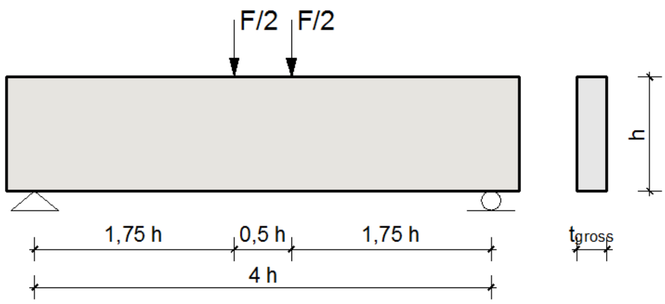

Figure 11. Geometry properties and test setup of test series E

All tests were run in deformation control. The rate of deformation was 0.03 mm/s for test series A and C, while for test series B and E the rate of deformation was 0.02 mm/s and for test series D the rate of the deformation was 0.01 mm/s. The chosen rates of deformation resulted in test durations of approximately 15-20 minutes. The rate of deformation referred to is the rate of the actuator in the testing machine. These rates of deformations allowed careful observations of critical corners and other locations on the specimens where cracks were expected, which enabled careful investigations on the initiation and propagation of cracks. However, in most of tested CLT beams initiation of the cracks were often somewhere inside the beam. The main reason for that is the specific layup of the tested CLT beams since, in most cases, failure was governed by shear stresses in the crossing areas between orthogonally bonded lamellae. In that sense, for most of the tested beams it was difficult to capture the first initiation of cracks because it was invisible by the naked eye from the outside of the beam and therefore only different sounds and leaps or load drops on graphs were observed and reported.

The following variables were recorded for all tests: the total deformation, the total applied load F, beam deflection δ and vertical/horizontal deformations d in the beam around holes and notches. In case of test series A, a total of 5 potentiometers were used to measure deformations, one on each side of the beam at the two tensile corners of the hole and a fifth one to measure the beam deflection δ (Fig. 12). In case of test series B, a total of 7 potentiometers were used to measure deformation. 4 potentiometers were used to measure the deformation at the two tensile corners of the hole from both sides, 2 potentiometers were placed on the front side of the beam at two compression corners of the hole and one sensor was used to measure the beam deflection δ at the location shown in Fig. 13.

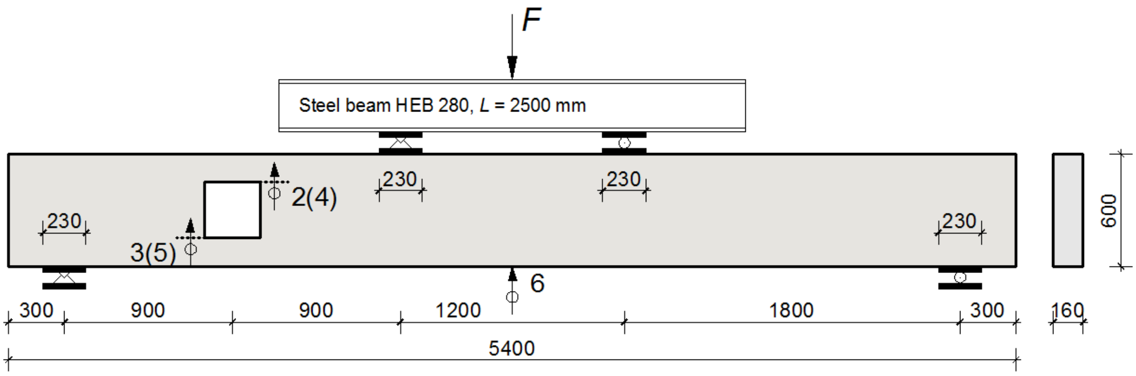

Figure 12. Test setup with dimensions, positions and labels of potentiometers for test series A (labels in brackets refer to the back face of the beam)

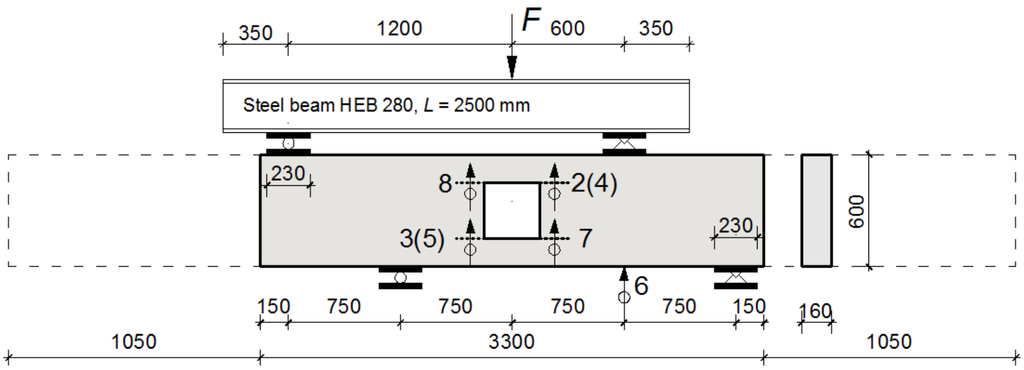

Figure 13. Test setup with dimensions, positions and labels of potentiometers for test series B (labels in brackets refer to the back face of the beam)

For test series C a total of 4 potentiometers were used. One potentiometer was used under the beam to measure the global beam deflection δ in the middle of the span, 2 potentiometers were used to measure deformation at supports and the last one was used to measure local deflection in the region with pure moment, between the two load application points. According to the test standard (EN 408), local and global MOE were calculated based on the measured global and local deflection. Further evaluation of local and global MOE is omitted in this report and will be published in further work. In case of test series D, a total of 7 potentiometers were used, where 4 potentiometers were used on each side of the beam at the two positions at the notch of the beam (Fig. 15), 2 potentiometers were used at supports and the last one was used to measure the beam deflection δ under the beam. For the last series, E, in total 7 potentiometers were used. According to the test standard (EN 308), potentiometers were positioned to measure shear deformations between one of the supports and the load application point (Fig. 16). However, like measured values of local and global MOE for test series C, further evaluation and description of measured shear modulus G is also omitted in this report but will be presented in future publications.

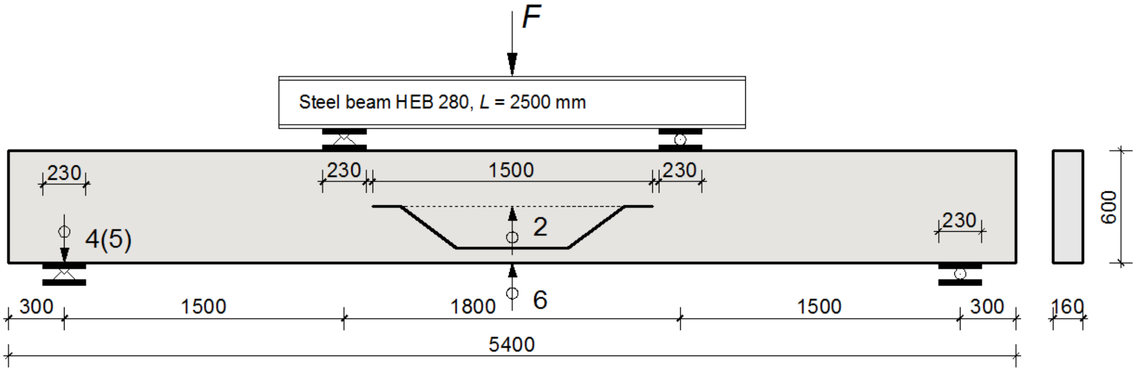

Figure 14. Test setup with dimensions, positions and labels of potentiometers for test series C (labels in brackets refer to the back face of the beam)

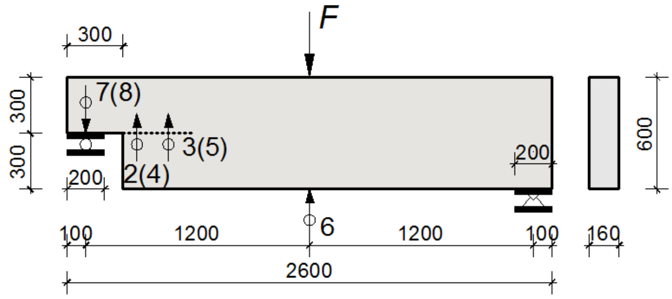

Figure 15. Test setup with dimensions, positions and labels of potentiometers for test series D (labels in brackets refer to the back face of the beam)

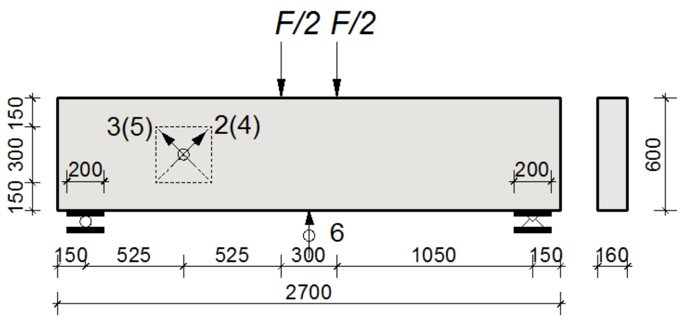

Figure 16. Test setup with dimensions, positions and labels of potentiometers for test series E (labels in brackets refer to the back face of the beam)

The placement of the potentiometers with labels indicating the measurement lengths is depicted in Figure 17. In all test series the measurement length was set to 100 mm, while distances d_1 and d_2 were changed depending on the dimensions of the outside longitudinal boards and the location of gaps between boards. In most cases, it was intended to measure the deformation d within a single longitudinal board. For this reason, different values of d_1 and d_2 were used as presented in Table 2. For test series D (notched CLT beams), two potentiometers were used at each side at the notch of the beam (Fig. 17).

Table 2. Dimensions of measure length of potentiometers for test series A, B and D

Test series	Number of specimen	d_1 [mm]	d_2 [mm]	d_3 [mm]	d_4 [mm]
A	1	50	50	50	-
	2	50	50	50	-
	3	50	50	50	-
	4	50	50	50	-
B	1	60	40	50	-
	2	70	30	50	-
	3	70	30	50	-
	4	70	30	50	-
D	1	50	50	15	70
	2	50	50	15	70
	3	50	50	15	70
	4	50	50	15	70

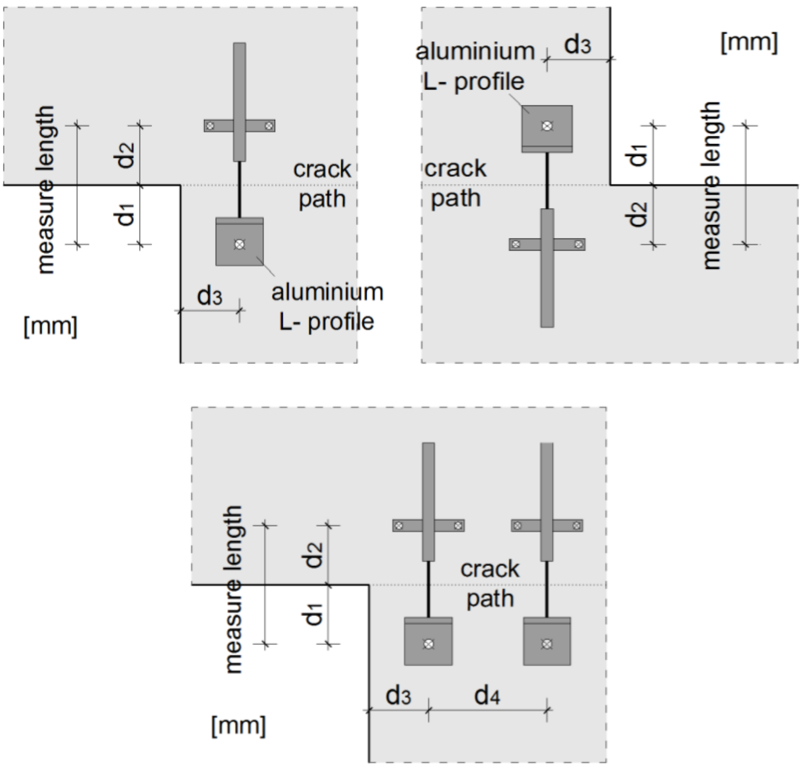

Figure 17. Placement of potentiometers for measurement of deformation d of test series A and B (left top – top corner, right top – bottom corner) and test series D (bottom)

Photos of the placement of potentiometers are shown in Figure 18. Photos of the test setups are shown in Figure 19. All tested beams were stabilized in the weak direction by means of roller supports at 1-3 locations along the beam (Fig. 19).

Figure 18. Photos of the potentiometers from test series A (top left), test series D (top right), test series B (middle left - front face, middle right - back face), test series C (bottom left) and test series E (bottom right)

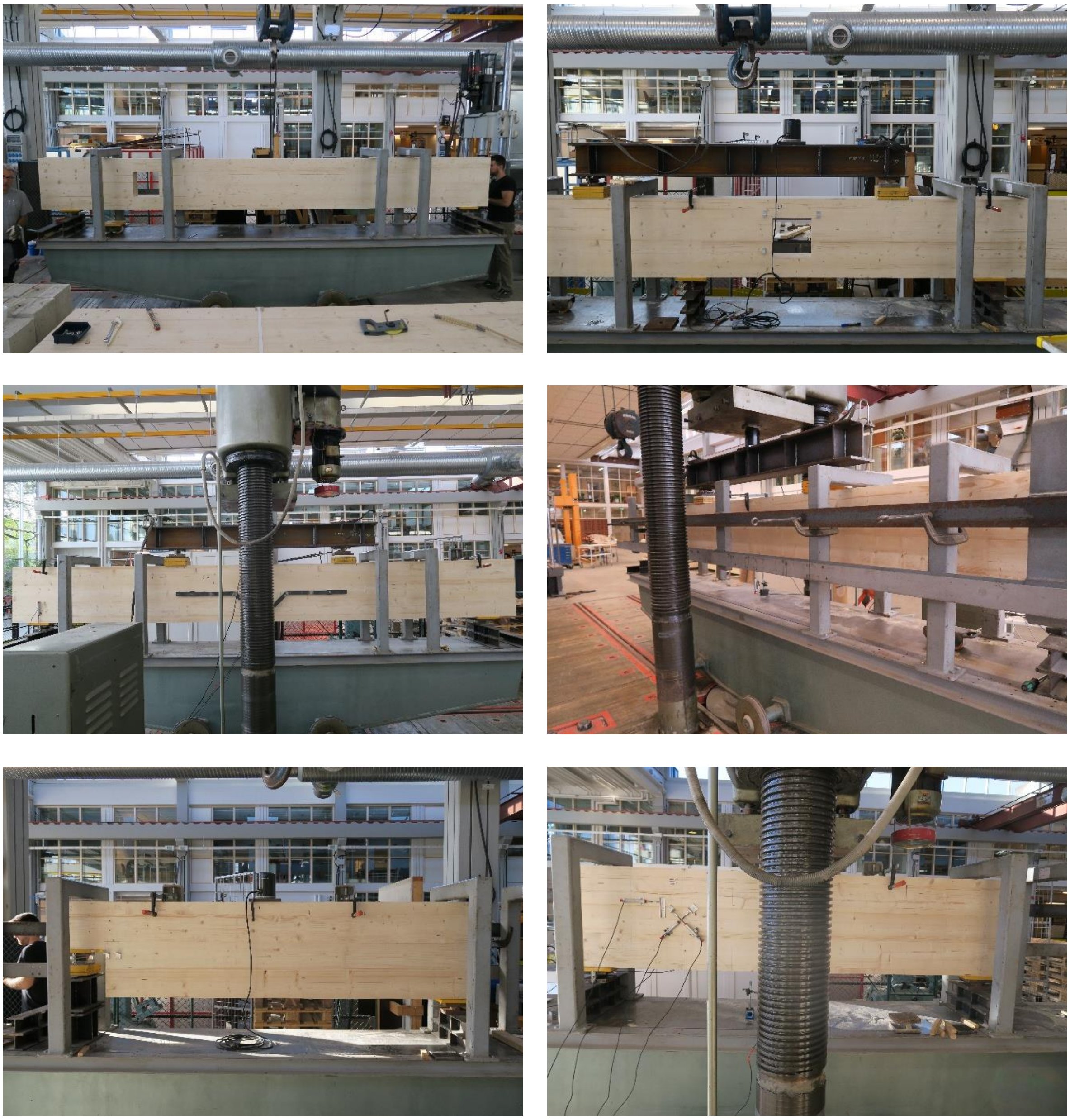

Figure 19. Photos of the test setups used for test series A (top left), test series B (top right), test series C (middle left - front face, middle right - back face), test series D (bottom left) and test series E (bottom right)

3.3. Materials and cross section layup

All tested beams were produced and delivered by Cross Timber Systems LTD. The beams were made of spruce (Lat. *Picea Abies*), glued with melamine-urea-formaldehyde resin and delivered with pre-made holes and notches. According to the manufacturer's specifications (ETA-15/0906, 2016.) for visually graded beams, at least 90 % of the boards were C24 strength class with each layer of the beams containing up to a maximum of 10 % of C16 strength class boards. Due to the specific layup of the tested beams, longitudinal and transversal boards were only glued over wide faces, meaning only within crossing areas, without gluing on the narrow faces of two adjacent boards within the same layer. The beams were produced in "standard" cross section layup containing in total 5 layers, with three layers in the longitudinal direction and two layers in the transversal direction. The lamellae thickness of the longitudinal layers was 40 mm and lamellae thickness of the transversal layers was 20 mm resulting in a total, or gross, thickness of 160 mm. The width of the individual longitudinal and transversal lamellae were different. The width of the longitudinal boards was 172 mm and the width of the transversal boards was 146 mm. Since the delivered beams were cut from large dimension CLT panels, the width of the longitudinal boards in the outermost layers of the beams was hence different for the different specimens. The actual measured cross section and board dimensions of each tested CLT beam is illustrated in Figure 20 to Figure 23. From the presented illustrations, only small differences can be noted regarding complete beam height. There are however large differences in the height of the outermost boards in the longitudinal layers, due the process of cutting the beams from large CLT panels.

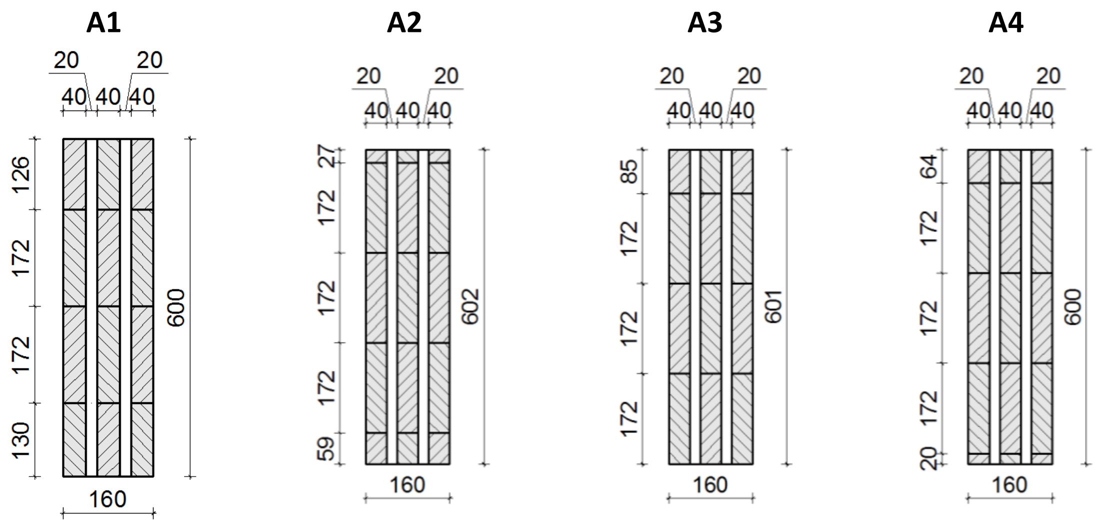

Figure 20. Dimensions of cross sections of four tested specimens form test series A (dimensions in mm)

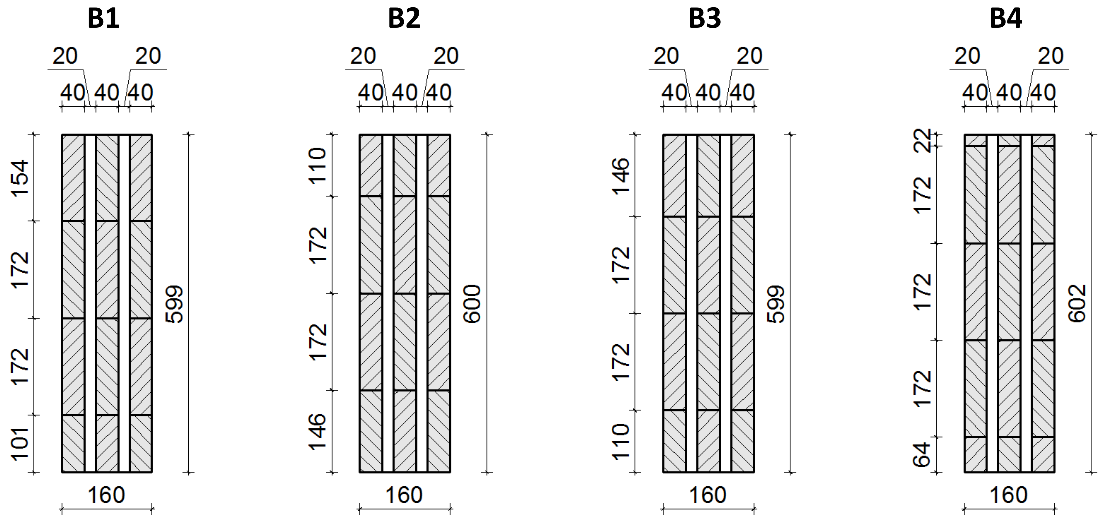

Figure 21. Dimensions of cross sections of four tested specimens form test series B (dimensions in mm)

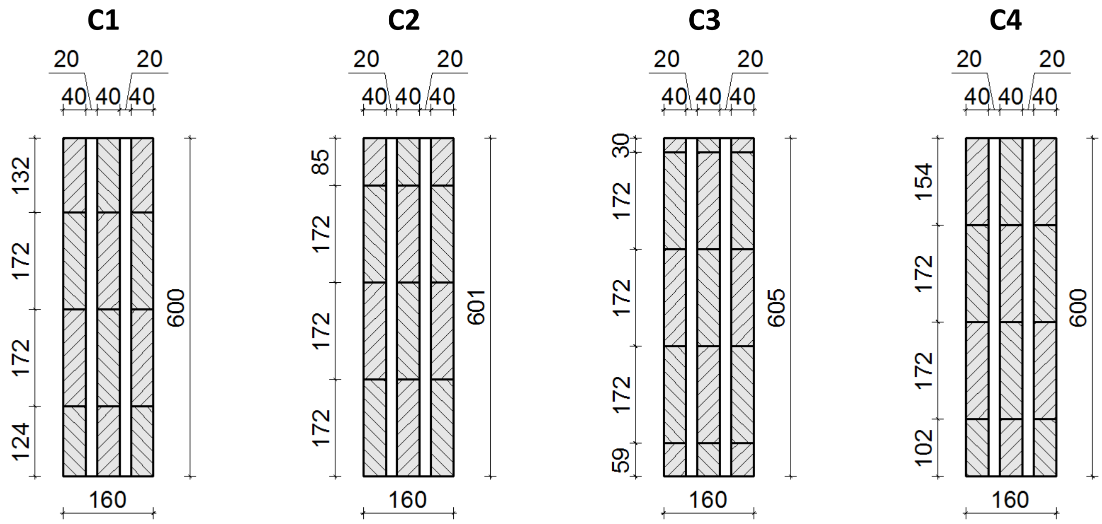

Figure 22. Dimensions of cross sections of four tested specimens form test series C (dimensions in mm)

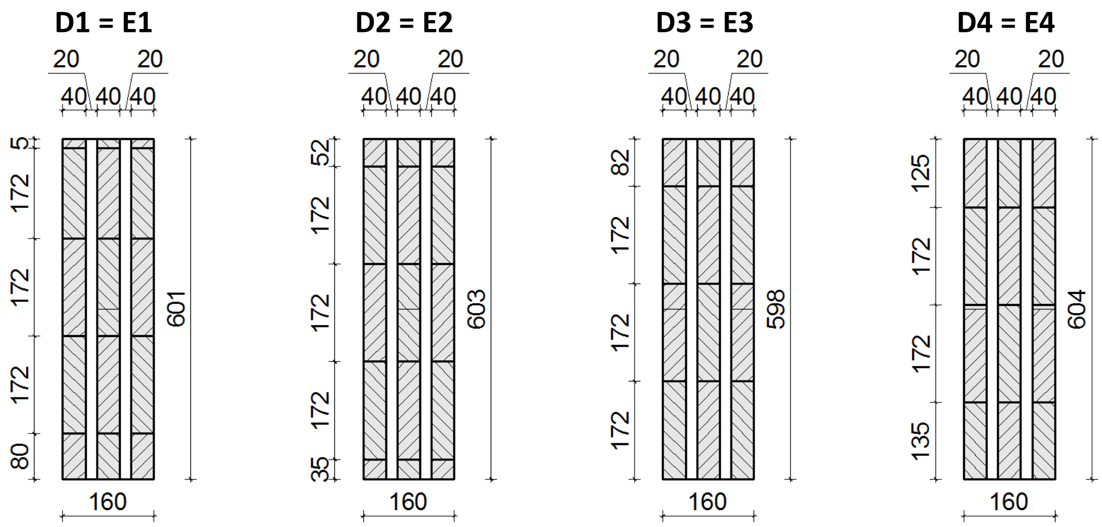

Figure 23. Dimensions of cross sections of four tested specimens form test series D and E (dimensions in mm)

The beams were delivered with a moisture content of approximately 12%. From the time of delivery to the time of testing the beams were kept indoors in a climate about 20°C and 35 % RH. The moisture content u at the time of testing was measured by an electric device at three different locations along each tested specimen resulting in average moisture content of all specimens under 12%. Additional calculation of moisture content u as well as the density ρ of material will be determined from smaller pieces of the tested beams. For this purpose, pieces of length of about 100 mm and width equal to the beam width were cut from each tested specimen. From measured mass and volume it is possible to obtain density and moisture for dry and test condition, respectively. Since these data are not processed yet, they are omitted in this report but will be included in future publications.

3.4. Results

The results are presented in the following way. The graphs and diagrams are firstly presented for each of the tested specimen including measurement of deflections δ under the beam, as well as deformations d measured around holes and notches. After that, photos of fractured specimens are shown with indications of possible failure modes of each tested specimen. In the next part the obtained maximum loads are compared with predicted beam strength values according to Flaig´s models, reviewed above. The final part of the presentation of results contains comparison between calculated critical stresses from maximum loads by using the analytical model from Flaig with corresponding strengths in relation to different failure modes.

The force F is plotted vs the beam deflection δ in Figure 24 for all individual tests. From these graphs similar values of the stiffness for each specimen from one tested series may in general be noticed. Except stiffness, values of maximum loads for each tested specimen from one series are also rather close, resulting in a small variation between results. In case of failure modes, from the presented graphs, higher variation may be noticed. The shape of the graph for some specimens is almost completely linear, indicating brittle failure after reaching maximum load, which was caused in most cases due to a bending type of failure, while for some specimens the shape of the graphs are characterized by a more elastic-plastic type of behavior indicating more ductile failure. Moreover, within one tested series, some specimens are characterized with completely different failure modes. Also, in some of the tested beams it was difficult to distinguish different failure modes, since in some cases they occur simultaneously.

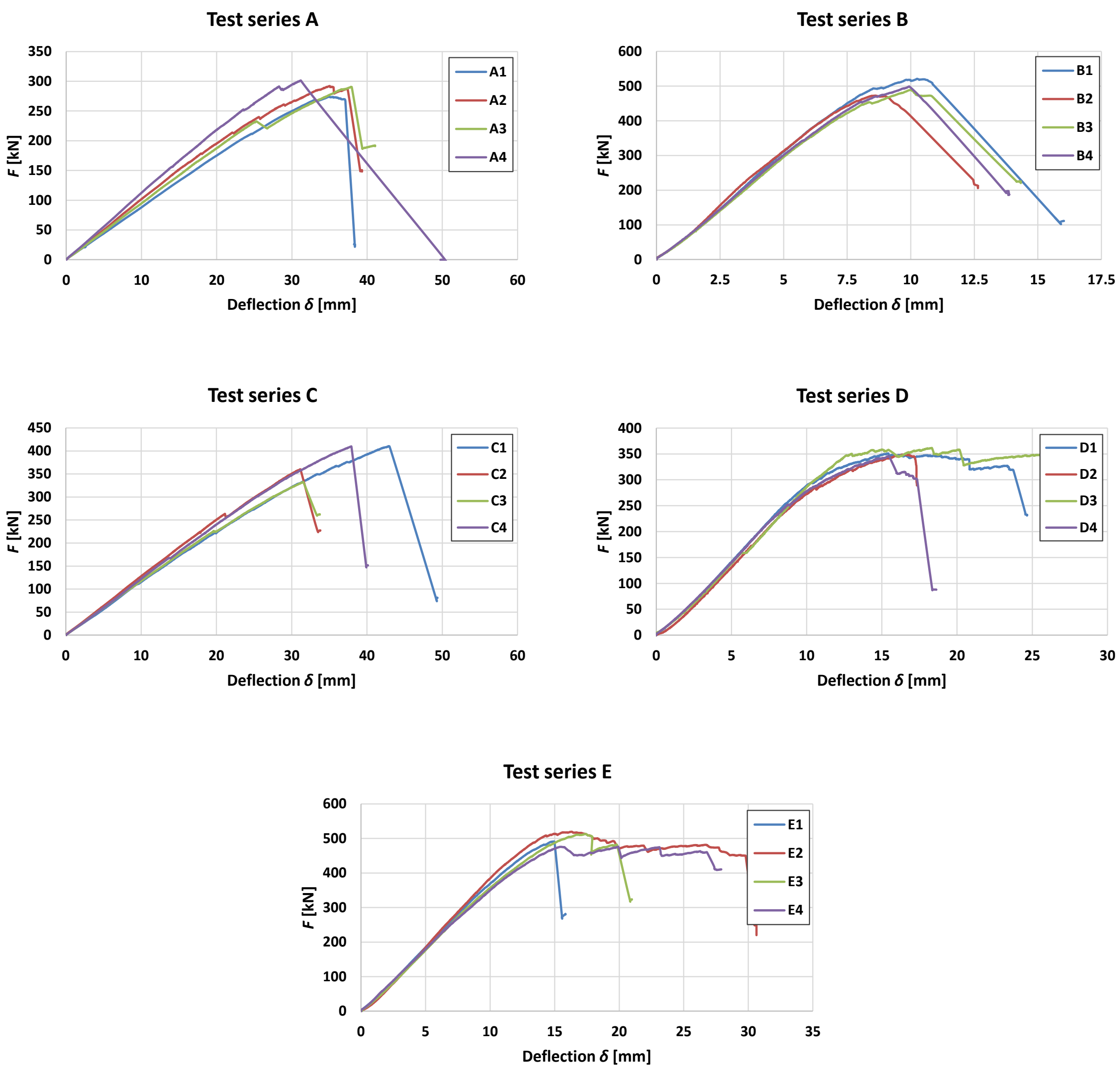

Figure 24. Diagrams of force F vs deflection δ for all tested test series

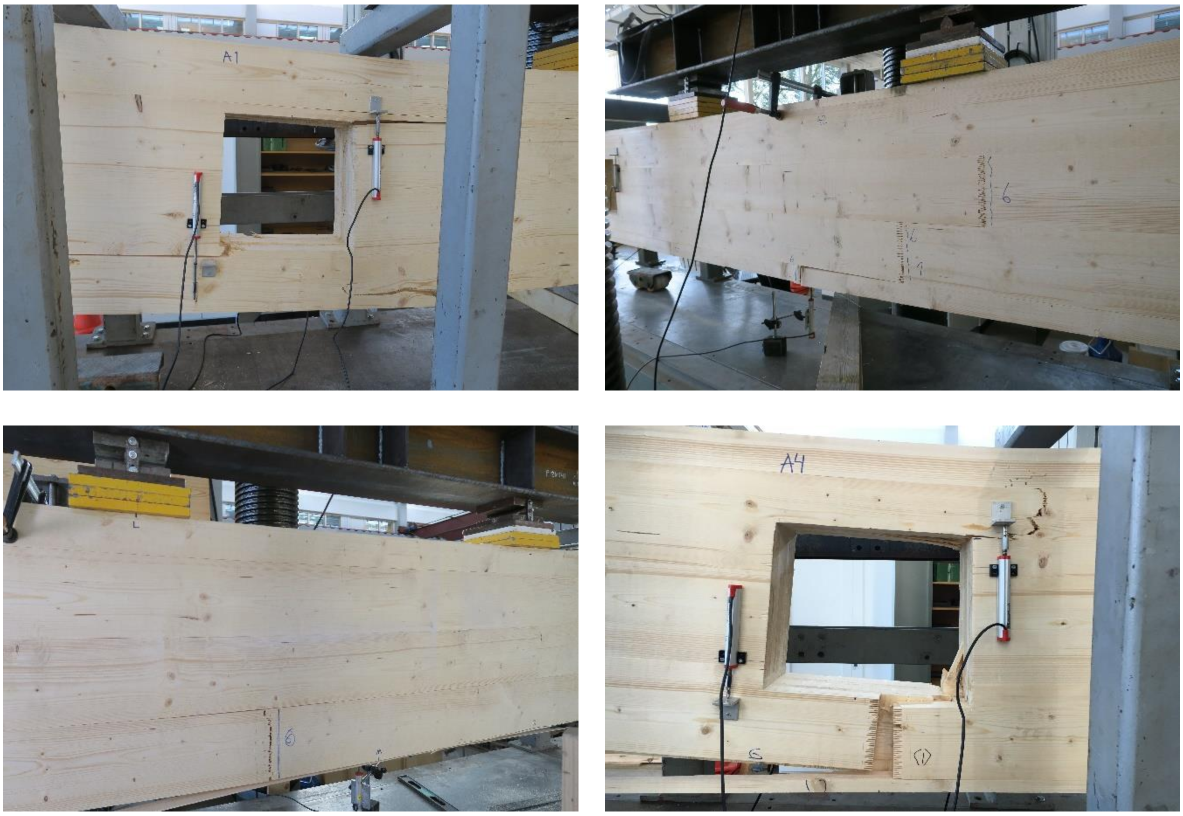

Figure 25. Photos of fractured specimens from test series A
(top left A1, top right A2, bottom left A3 and bottom right A4)

Figure 26. Photos of fractured specimens from test series B
(top left B1, top right B2, bottom left B3 and bottom right B4)

Figure 27. Photos of fractured specimens from test series C
(top left C1, top right C2, bottom left C3 and bottom right C4)

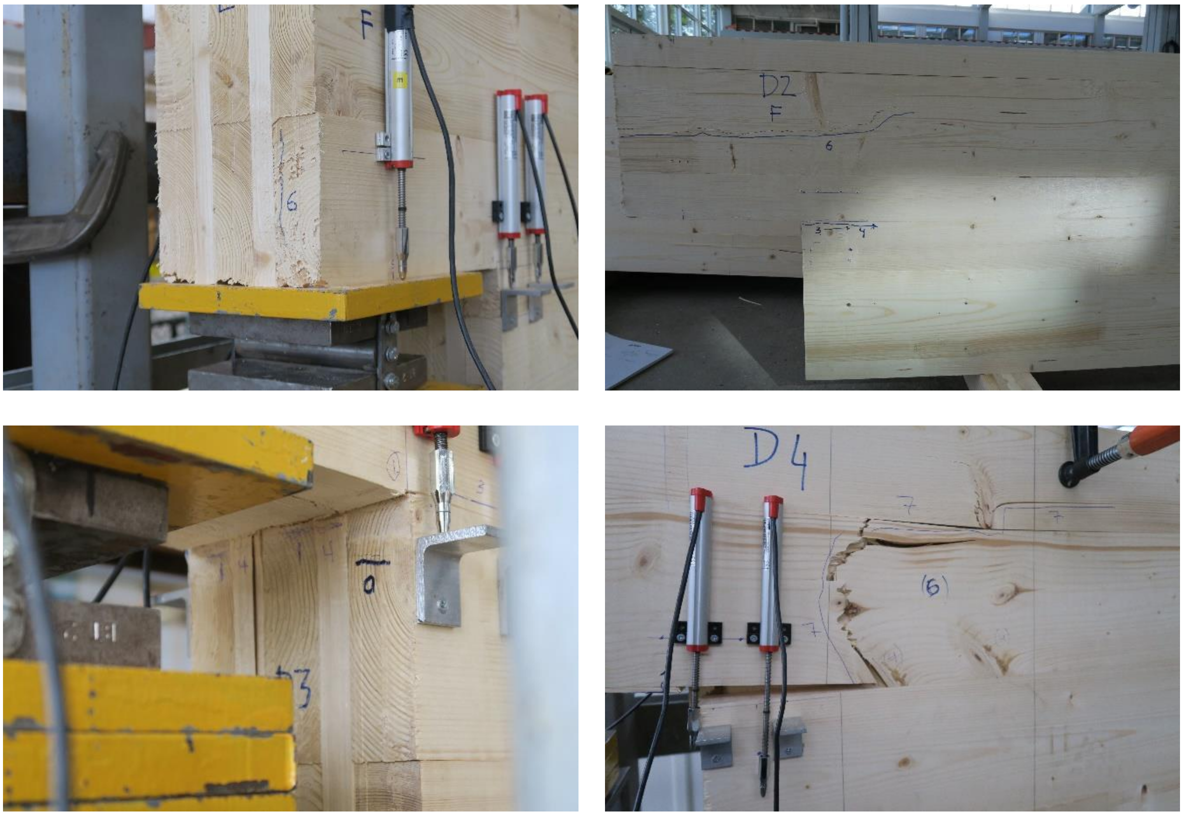

Figure 28. Photos of fractured specimens from test series D
(top left D1, top right D2, bottom left D3 and bottom right D4)

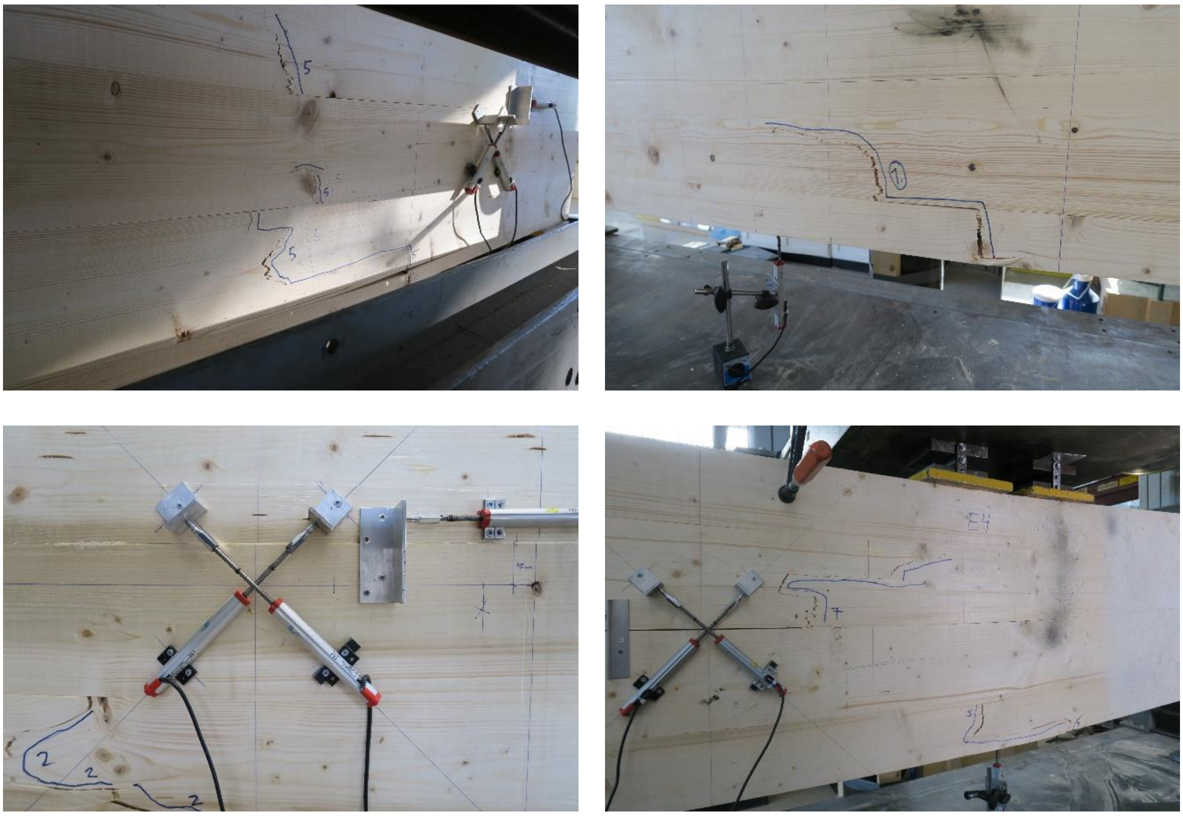

Figure 29. Photos of fractured specimens from test series E
(top left E1, top right E2, bottom left E3 and bottom right E4)

The force *F* is plotted vs the deformation *d* in Figures 30 to 32 for test series A and B with holes and test series D with notches. Positions and labels of potentiometers are shown in Figures 12 to 15 for each of the test series. In case of test series A and B, deformations were measured around the holes from both faces of the beam and in case of test series D from both faces at the notch of the beam. For test specimen A3 and B5, measurements were performed only from the back side of the beam (potentiometer 4 and potentiometer 5) since on the front side a DIC-measuring system was used. Since these data are not processed yet, they are omitted in this report but will be included in future publications. In figures 30 to 31, blue lines represent deformations measured on top tensile corners and red lines on bottom tensile corners. In figure 32, blue lines represent potentiometer closer to the notch and red lines further from the notch. The solid lines represent measurement from the front side of the beam and dotted lines from the back side of the beam.

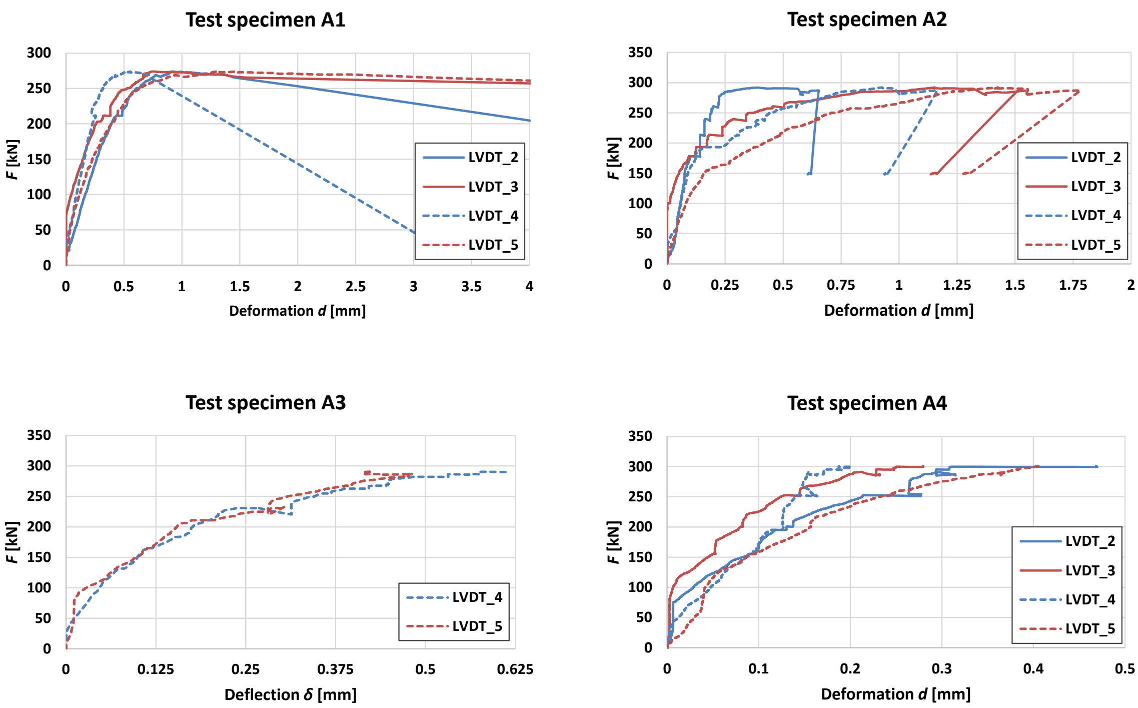

Figure 30. Diagrams of force F vs deformation d for test series A

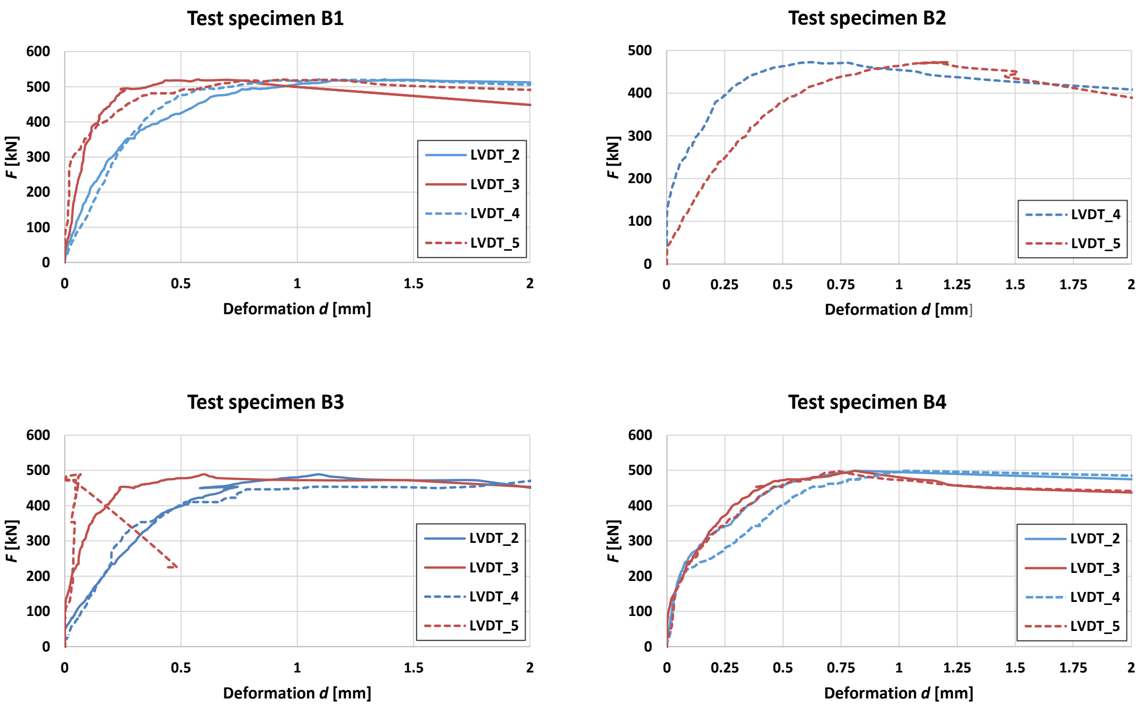

Figure 31. Diagrams of force F vs deformation d for test series B

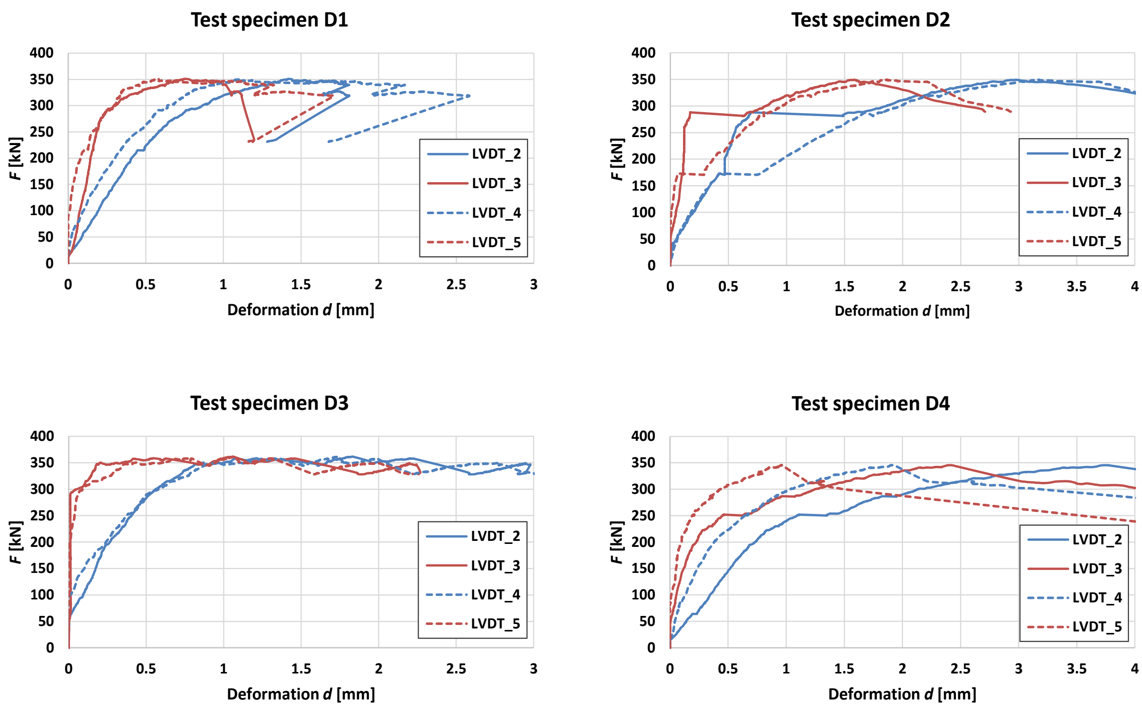

Figure 32. Diagrams of force F vs deformation d for test series D

In table 3, results in terms of obtained maximum loads *F* for each of the tested specimens are presented. In addition to the individual results for each specimen mean values, standard deviations and coefficient of variations are given for each of test series.

Table 3. Experimental obtained failure load F in [kN]

Number of specimen	Test series A	Test series B	Test series C	Test series D	Test series E
1	274	520	410	350	491
2	291	472	360	349	519
3	290	488	332	361	512
4	301	499	409	345	476
Mean	**289**	**495**	**378**	**351**	**500**
Std [kN]	11.3	20.2	38.4	6.90	19.8
CoV [%]	3.90	4.09	10.1	1.96	3.98

In table 4, the predicted load carrying capacities according to Flaig´s analytical model are presented. For each failure mode, load carrying capacity or maximum load *F* was calculated using assumed mean values of the corresponding strengths for timber class C24 (Table 5).

Furthermore, the predicted failure loads according to Flaig’s model were determined based considering a simplified and symmetric cross section layup in terms of the individual board dimensions according to Fig. 33. The simplified cross section is composed of four longitudinal lamellae of (equal) height of 150 mm which equals to the nominal height of 600 mm. Also the height of the transversal lamellae was assumed as 150 mm. Since Flaig´s equations, reviewed above, are based on equal widths of longitudinal and transversal lamellae, a width of 150 mm was used as an average value for all lamellae of each tested beam.

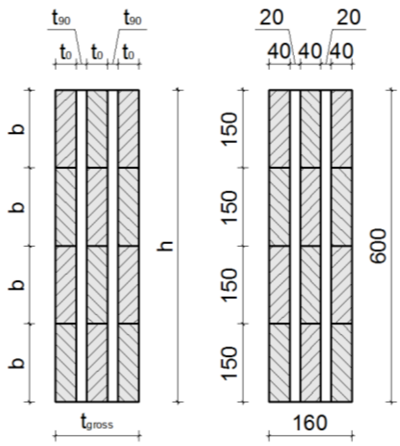

Figure 33. Nominal notations and dimensions of cross section of CLT beam (dimensions in mm)

Table 4. Predicted failure load F_{max} in [kN] based on nominal cross section of CLT beam

Failure mode	Test series A	Test series B	Test series C	Test series D	Test series E
Bending	280	1260	**336**	420	480
Bending at hole/notch	**210**	551	-	630	-
Tension perp. to the beam axis	525	905	-	323	-
FM I	320	480	640	320	640
FM II	237	**356**	400	**217**	**400**
FM III-A	247	371	463	-	463
FM III-B	265	420	-	306	-

Table 5. Assumed mean strength values of timber class C24 in MPa

Bending strength f_m	Compression parallel to the grain $f_{c,0}$	Tension parallel to the grain $f_{t,0}$	Shear strength parallel to the grain $f_{v,lam}$	Shear strength perpendicular to the grain $f_{v,lam,90}$	Torsional shear strength (FM III) $f_{v,tor}$	Rolling shear strength (FM III) f_R
35.0	30.0	35.0	5.00	12.5	3.50	1.50

In table 6 to 10, calculated critical stresses from maximum obtained load F_{max} for each of tested specimen are presented. Critical stresses that caused failure of the specimen are set in boldface and underlined. Calculation of critical stresses is based on the simplified cross section dimensions of CLT beams described above with one exception: for calculation of tension stresses perpendicular to the beam axis, the actual measured width of the first transversal lamellae near the hole or notch was used. The dimensions of the first transversal lamella b_{cross} are presented in each table for each specimen.

Table 6. Ultimate loads in [kN] and evaluated stresses and strengths in [MPa] for test series A

Critical stresses	A1	A2	A3	A4	Mean	Strength
F_{max}	274	291	290	301	289	-
$\sigma_{m,net}$	34.2	**<u>36.5</u>**	**<u>36.3</u>**	37.6	36.2	35.0
$\sigma_{m,net,h}$	**<u>45.6</u>**	48.6	48.4	**<u>50.2</u>**	48.2	35.0
$\sigma_{t,0,cross}$	18.7	21.1	19.9	24.9	21.2	35.0
$\tau_{xy,gross,h}$	4.28	4.56	4.54	4.71	4.52	5.00
$\tau_{xy,net,h}$	14.4	15.3	15.2	15.8	15.2	12.5
$\tau_{tor,h}$	2.18	2.33	2.32	2.40	2.30	3.50
$\tau_{xz,h}$	0.72	0.76	0.76	0.79	0.75	1.50
$\tau_{yz,h}$	0.61	0.70	0.66	0.83	0.70	1.50
b_{cross}*	146	138	146	121	-	-
Failure mode	Bending at hole	Bending at midspan	Bending at midspan	Bending at hole	-	-

**width of first vertical lamellae near the hole in [mm]*

Table 7. Ultimate loads in [kN] and evaluated stresses and strengths in [MPa] for test series B

Critical stresses	B1	B2	B3	B4	Mean	Strength
F_{max}	520	472	488	499	495	-
$\sigma_{m,net}$	18.1	16.4	16.9	17.3	17.2	35.0
$\sigma_{m,net,h}$	33.1	30.0	31.0	31.7	30.9	35.0
$\sigma_{t,0,cross}$	22.1	20.1	22.9	23.8	22.2	35.0
$\tau_{xy,gross,h}$	5.42	4.92	5.09	5.19	5.16	5.00
$\tau_{xy,net,h}$	18.2	16.5	17.1	17.5	17.3	12.5
$\tau_{tor,h}$	**<u>2.77</u>**	**<u>2.51</u>**	**<u>2.61</u>**	**<u>2.66</u>**	2.64	3.50
$\tau_{xz,h}$	0.91	0.83	0.86	0.87	0.87	1.50
$\tau_{yz,h}$	**<u>0.74</u>**	**<u>0.67</u>**	**<u>0.69</u>**	**<u>0.71</u>**	0.70	1.50
b_{cross}*	138	138	125	123	-	-
Failure mode	FM III-B	FM III-B	FM III-B	FM III-B	-	-

**width of first vertical lamellae near the hole in [mm]*

Table 8. Ultimate loads in [kN] and evaluated stresses and strengths in [MPa] for test series C

Critical stresses	C1	C2	C3	C4	Mean	Strength
F_{max}	410	360	332	409	378	-
$\sigma_{m,net}$	**42.7**	**37.5**	**34.6**	**42.6**	39.4	35.0
$\tau_{xy,gross}$	3.20	2.81	2.59	3.20	2.95	5.00
$\tau_{xy,net}$	12.8	11.2	10.4	12.8	11.8	12.5
τ_{tor}	1.60	1.41	1.30	1.60	1.47	3.50
τ_{xz}	0.64	0.56	0.52	0.64	0.59	1.50
Failure mode	Bending at midspan	Bending at midspan	Bending at midspan	Bending at midspan	-	-

Table 9. Ultimate loads in [kN] and evaluated stresses and strengths in [MPa] for test series D

Critical stresses	D1	D2	D3	D4	Mean	Strength
F_{max}	350	349	361	345	351	-
$\sigma_{m,net}$	29.2	29.1	30.1	28.8	29.3	35.0
$\sigma_{m,net,n}$	19.5	19.4	20.1	19.2	19.5	35.0
$\sigma_{t,0,cross}$	38.0	37.8	39.1	37.4	38.1	35.0
$\tau_{xy,gross,n}$	5.48	5.46	5.65	5.40	5.49	5.00
$\tau_{xy,net,n}$	20.1	20.1	20.8	19.8	20.2	12.5
$\tau_{tor,n}$	**2.52**	**2.51**	**2.60**	**2.48**	2.53	3.50
$\tau_{xz,n}$	-	-	-	-	-	1.50
$\tau_{yz,n}$	**0.63**	**0.63**	**0.65**	**0.62**	0.63	1.50
b_{cross}*	63	65	40	146		-
Failure mode	FM III-B	FM III-B	FM III-B	FM III-B	-	-

**width of first vertical lamellae near the notch in [mm]*

Table 10. Ultimate loads in [kN] and evaluated stresses and strengths in [MPa] for test series E

Critical stresses	E1	E2	E3	E4	Mean	Strength
F_{max}	491	519	512	476	500	-
$\sigma_{m,net}$	**35.1**	**37.9**	**37.4**	**34.7**	36.4	35.0
$\tau_{xy,gross}$	3.84	4.06	4.00	3.72	3.91	5.00
$\tau_{xy,net}$	15.3	16.2	16.0	14.9	15.6	12.5
τ_{tor}	1.91	2.02	2.00	1.86	1.95	3.50
τ_{xz}	0.76	0.81	0.80	0.74	0.78	1.50
Failure mode	Bending at midspan	Bending at midspan	Bending at midspan	Bending at midspan	-	-

4. Conclusions

Some comments and general conclusions on the test results concerning each tested series are listed below.

Test series A

All test specimens from test series A failed in bending. Two of them failed in bending at the hole and the other two in bending at midspan. It seems like the proposed model underestimates shear capacities of CLT beams with a hole regarding shear failure mode FM II and FM III. Possible reasons can be the used stress concentration factors. Another possible reason can be the assumed mean values of the lamellae strengths being too low.

Test series B

All test specimens from test series B failed in shear failure mode FM III-B within crossing areas around the two tensile corners of the hole. According to the analytical predictions, the critical failure mode should be FM II or FM III-A which indicates that the FM II shear capacity of the CLT beams is underestimated. The analytical model underestimations could be caused by too high stress concentration factors or too low mean value of shear strength perpendicular to the grain $f_{\text{v,lam,90}}$.

However, characterization of the critical failures as failure mode FM III-B is based solely on general observations during testing and analysis of the behavior of the load vs deflection relationship, since initiation of failure was inside the beam and no obvious cracking could be seen from the outside until the final stage. DIC measuring equipment was used for one tested specimen and the results will be evaluated and presented in future publications.

Test series C

All test specimens from test series C failed in bending at midspan. For this test series, the coefficient of variation was the highest (10.2 %) among all test series. Local and global MOE were also measured according to the standard EN 408. In future publications, these results will be evaluated and presented.

Test series D

All test specimens from test series D failed in shear failure mode FM III at the notch of the beam. Initiation of failure started inside the beam in crossing areas indicating FM III-B as critical failure mode. However, final failure was characterized as combination of failure mode FM III-B and FM I, meaning gross shear failure in the part of the beam above the notch. Also, interesting behavior in terms of considerable load bearing capacity after reaching maximum load was found for some of the tests (see Fig. 24). Since only four specimens were tested, it is not possible to make any general conclusions with respect to the width of the first transversal lamellae near the notch. In the tested beams, that dimension varied from 40 mm to 146 mm without any major difference in behavior of the beam.

Test series E

Test series E was designed in order to test the shear strength and the shear stiffness of the CLT beams, using a test configuration according to proposal by Gehri, 2003. However, for all tested specimens the final failure was caused by bending. Still, from the presented graphs it seems like at least some partial shear failure occurred in some of tested beams since the stiffness seems to decrease at load levels of about 400 kN and since large sliding between longitudinal boards was visible during testing. Furthermore, three out of the four tests show significant load bearing capacity after reaching maximum load and before the final stage of failure. Like in the previous test series, underestimation of shear capacities related to FM II and FM III is again emphasized.

5. References

Blass, H-J, Ehlbeck, J, Kreuzinger, H, Steck, G (2004): Erläuterungen zur DIN 1052:2004-08; Entwurf, Berechnung und Bemessung von Holzbauwerken. 2. Aufgabe; DGfH Innovations – und service GmbH, München.

Bogensperger, T, Moosbrugger, T, Silly, G (2010): Verification of CLT-plates under loads in plane. In: Proc. 11th World Conference on Timber Engineering, Riva del Garda, Italy.

Bogensperger, T, Moosbrugger, T, Schickhofer, G (2007): New Test Configuration for CLT-Wall Elements under Shear Load. In: Proc. CIB-W18 Meeting 40, Bled, Slovenia, Paper 40-12-3.

Brandner, R, Bogensperger, T, Schickhofer, G (2013): In plane Shear Strength of Cross Laminated Timber (CLT): Test Configuration, Quantification and influencing Parameters. In: Proc. CIB-W18 Meeting 46, Vancouver, Canada, Paper 46-12-2.

Brandner, R, Flatscher, G, Ringhofer, A, Schickhofer, G, Thiel, A (2016): Cross laminated timber (CLT): overview and development. European Journal of Wood and Wood Products, 74:331-351.

Danielsson, H (2007): The Strength of Glulam Beams with Holes – A Survey of Tests and Calculation Methods. Report TVSM-3068, Division of Structural Mechanics, LTH, Lund University.

DIN EN 1995-1-1/NA (2013) National Annex – Nationally determined parameters – Eurocode 5: Design of timber structures – Part 1-1: General – Common rules and rules for buildings.

EN 16351 (2015) Timber structures – Cross laminated timber – requirements (CEN).

EN 408 (2012) Timber Structures – Structural timber and glued laminated timber – Determination of some physical and mechanical properties (CEN).

ETA-12/0281, "NORITEC X-LAM" (2012): Cross Laminated Timber (CLT) – Solid wood slab elements to be used as structural elements in buildings", NORITEC Holzindustrie GmbH, Österreichisches Institut für Bautechnik (OIB).

Eurocode 5 (2004): Design of timber structures - Part 1-1: General and rules for buildings. European Committee for Standardization (EN 1995-1-1)

Flaig, M (2015): In Plattenebene beanspruchte Biegeträger aus Brettsperrholz. Bautechnik, 92:741-749.

Flaig, M (2014): Design of CLT Beams with Rectangular Holes or Notches, In: Proc. 1st INTER Meeting, Bath, United Kingdom, Paper 47-12-4.

Flaig, M, Blass, H-J (2013): Shear strength and Shear stiffness of CLT beams loaded in plane. In: Proc. CIB-W18 Meeting 46, Vancouver, Canada, Paper 46-12-3.

Flaig, M (2013): Biegeträger aus Brettsperrholz bei Beanspruchung in Plattenbene. Dissertation, Karlsruher Berichte zum Ingenieurholzbau, Bd. 26, KIT Scientific Publishing

Gehri, E (2010): Shear problems in timber engineering – Analysis and solutions. In: Proc. 11th World Conference on Timber Engineering, Riva del Garda, Italy.

Jelec, M, Rajcic, V, Danielsson, H, Serrano, E (2016): Structural analysis of in-plane loaded CLT beams with holes: FE-analyses and parameter studies, In: Proc. 3rd INTER Meeting, Graz, Austria, Paper 49-12-2.

Moosbrugger, T, Guggenberger, W, Bogensperger, T (2006): Cross Laminated Timber Wall Segments under homogeneous Shear – with and without Openings. In: Proc. 9th World Conference on Timer Engineering, Portland, Oregon, USA.

ÖNORM B 1995-1-1/NA (2014) National Annex – Nationally determined parameters – Eurocode 5: Design of timber structures – Part 1-1: General – Common rules and rules for buildings.

Serrano, E (2016): Rational modelling and design in timber engineering applications using fracture mechanics. In: Proc. 14th World Conference on Timber Engineering, Wiena, Austria.

Schickhofer, G, Bogensperger, T, Moosburger, T (2010): BSPhandbuch (CLThandbook: solid timber construction technique with cross laminated timber – verification base on new European standardization concept). Verlag der Technischen Universität Graz (in German).

6. Appendix

LUND UNIVERSITY

2016-11-10

To whom it may concern

Structural Mechanics
Erik Serrano, professor
Head of division

COST FP1402 - Confirmation regarding STSM

Mr Mario Jelеč has, during a stay at Lund University, Div. of Structural Mechanics, successfully accomplished a short term scientific mission (STSM). The STSM has been performed during the period 2016-08-31 – 2016-10-14.

During his stay, Mr. Jeleč has been supervised by Dr. Henrik Danielsson and myself. The work performed has contributed in general to our knowledge about CLT, and in particular to our knowledge about the use, testing and modelling of CLT beams. Mr. Jelec has shown excellent collaboration skills, skills in experimental and numerical methods and has shown a great engagement in his work. We look forward to a continued and fruitful collaboration in the future.

On behalf of the host institution,

Erik Serrano
Professor, Head of Division

Postal address	Visiting address	Telephone	Fax	E-mail	Website
PO Box 118	John Ericssons väg 1	+46 46 222 03 19	+46 46 222 44 20	erik.serrano@construction.lth.se	www.byggmek.lth.se
SE 221 00 LUND	SE 223 63 LUND	+46 46 222 00 00			